4-5-2007

On Comparison of Indentation Models

John Louis Daly Jr.
University of South Florida

On Comparison of Indentation Models

by

John Louis Daly, Jr.

A thesis submitted in partial fulfillment
of the requirements for the degree of
Master of Science in Mechanical Engineering
Department of Mechanical Engineering
College of Engineering
University of South Florida

Major Professor: Autar Kaw, Ph.D.
Daniel Hess, Ph.D.
Craig Lusk, Ph.D.

Date of Approval:
April 5, 2007

Keywords: functionally gradient materials, FEA, ANSYS, parabolic contact problem, Hertzian contact model

Dedication

This thesis is dedicated to my parents, to my grandmother, and to Dr. Autar Kaw who believed in me through the most difficult times in my life and provided support far beyond that which was expected of them.

Acknowledgements

Thanks to my parents and my grandmother for helping me get by every single day and to my sister and her family for taking care of me and cooking the world's best pot roast when my parents were out of the country.

A special thanks to Dr. Autar Kaw not only for his support throughout graduate school, but also for his amazing insights into solid mechanics, complicated mathematics, programming, and pop culture. Dr. Kaw has been a teacher, a role model, and a friend to me. I would also like to thank Dr. Glen Besterfield who has been a great inspiration and who helped get me started in graduate school. I hope that someday he will return to the Department of Mechanical Engineering

I would like to thanks to Ms. Sue Britten who, during my entire time in engineering at USF, has always been in a good mood and extremely helpful. Her contribution to the students in this department over the years has been immeasurable.

Thanks to friends Kimberly, Rob, Emmett, Nathan, Billy, James, Phaninder, Saurabh, Jimmie, Abraham, Daniel, Lucas, and all three J. Russel's.

I would also like my committee members Dr. Daniel Hess and Dr. Craig Lusk for their contributions and for being on my committee.

Table of Contents

List of Tables

List of Figures

List of Nomenclature

σ_{yy}	*y* normal stress
σ_{xy}	*x-y* shear stress
$\sigma_{yy}(h)_{max}$	Max. *y* normal stress in the homogeneous model
$\sigma_{yy}(nh)_{max}$	Max. *y* normal stress in the nonhomogeneous model
$\sigma_{xy}(nh)_{max}$	Max. *x-y* shear stress in the nonhomogeneous model
$\sigma_{xy}(h)_{max}$	Max. *x-y* shear stress in the homogeneous model
v	Displacement in y
$v\ (h)_{max}$	Max. *y*-disp. in the homogeneous model
$v\ (nh)_{max}$	Max. *y*-disp. in the homogeneous model
a	contact length
E_1	Maximum modulus of the film
E_2	Modulus of the substrate
E_i	Modulus of a film layer
h	Thickness of a single film layer
H	Model height
T_f	Thickness of the film
R	Radius of the indenter

On Comparison of Indentation Models

John Louis Daly, Jr.

ABSTRACT

Thin films that are functionally gradient improve the mechanical properties of film-substrate layered materials. Mechanical properties of such materials are found by using indentation tests. In this study, finite element models are developed to simulate the indentation test. The models are based on an axisymmetric half space of a specimen subjected to spherical indentation. The film layer through the thickness is modeled to have either homogeneous material properties or nonhomogeneous material properties that vary linearly.

Maximum indenter displacement, and maximum normal and shear stresses at the interface are compared between the homogeneous model and the nonhomogeneous model for pragmatic contact length to film thickness ratios of 0.2 to 0.4, and film to substrate moduli ratios of 1 to 200 to 1.

Additionally, a coefficient is derived from regression of the stress data produced by these models and compared to that used to define the pressure field in the axisymmetric Hertzian contact model. The results of this study suggest

that a displacement boundary condition to an indenter produces the same results as a pressure distribution boundary condition.

The critical normal stresses that occur between modeling a film as a nonhomogeneous and as a homogeneous material vary from 19% for a modulus ratio of 2.5:1 to as high as 66% for a modulus ratio of 200:1 indicating that the modeling techniques produced very different maximum normal stresses. The difference in the maximum shear stress between the nonhomogeneous and the homogeneous models varied from 19% for a 2.5:1 modulus ratio to 57% for the 200:1 modulus ratio but reached values as low as 6% for the 50:1 modulus ratio. The maximum contact depth between the nonhomogeneous and the homogeneous models varied from 14% for the 2.5:1 case to as much as 75% in the 200:1 case.

The results from the reapplication of the pressure field derived from the regression coefficients and the R^2 values from these regression models indicate the correctness of the regression model used as well as its ability to replicate the normal stresses in the contact area and maximum indenter displacements in a FEA model for both the homogeneous and the nonhomogeneous models for modulus ratios ranging from 2.5:1 to 200:1.

The agreement between the regression based coefficients and the force based coefficients suggests the validity for the use of the theoretical axisymmetric Hertzian contact model for defining the pressure field in the contact area and displacements for both the homogeneous case and the

nonhomogeneous case for the considered film to substrate moduli ratios and contact length to film thickness ratios.

Chapter 1: Introduction

1.1 Functionally gradient materials

The natural world has historically challenged man by offering seemingly simplistic solutions to design challenges that often prove difficult to replicate through technology. Functionally gradient materials (FGM) are an example of this scenario. A material is said to be functionally gradient when its composition gradually varies throughout its volume. This gradual variation in material composition allows for the material properties of a body to vary greatly from the bulk structure of the material without experiencing interface problems that are found in abrupt interface composites. Through gradual transitions in material composition, a structure can benefit from both the properties of the substrate and the properties of the materials surface with a reduction of interface effects such as thermal stresses and bonding issue that can be found in the discrete bonding of dissimilar materials. In the natural world, functionally gradient materials can be observed in the structure of bamboo, the nanostructure of bones, and the material composition of most trees. The benefits of functionally gradient material properties have been exploited for years through the process of case hardening of steels. The initial concept and the development of this technology for dissimilar materials are credited to M. Niino at the National Aerospace Laboratory of Japan (R. Narayan, 2006). Niino's concept for the development of a FGM

coating was born from the need to provide a thermal barrier material for space vehicles and fusion reactors. Since then, this technology has found continual applications in the development of thermal coatings as well as applications in mining, and bearing surfaces in human joint replacements.

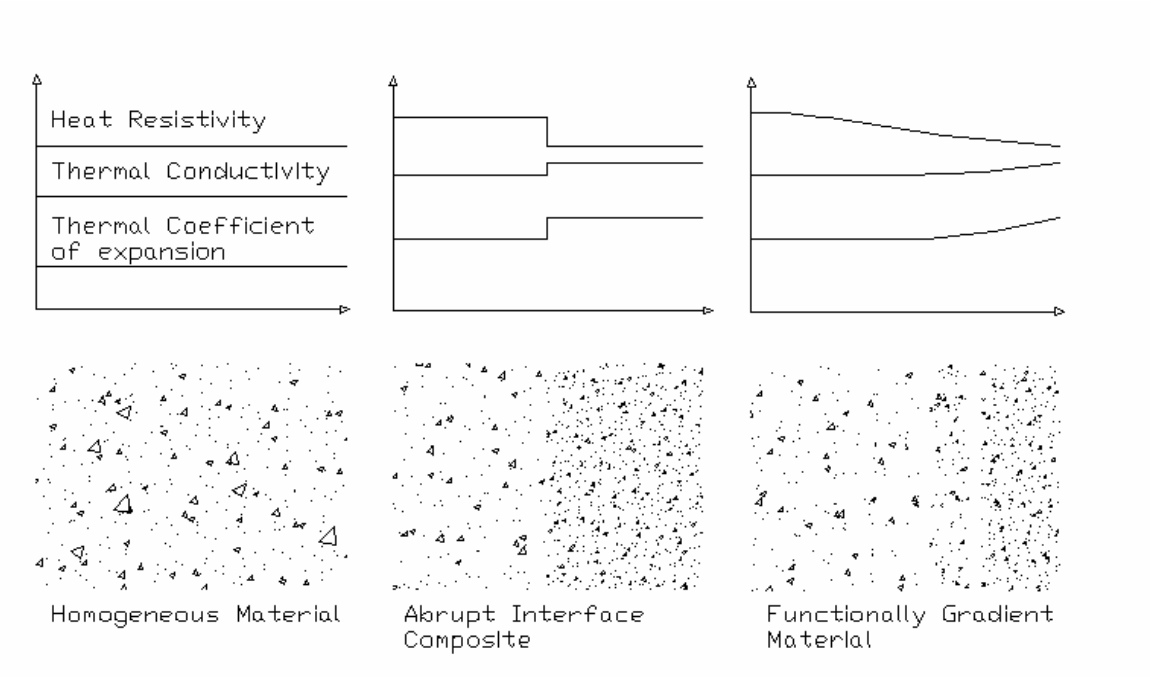

Figure 1: Material property comparison of abrupt interface composites and functionally gradient materials

1.2 Spherical indentation

With the ongoing use of these types of materials in technological applications comes the need for continual improvement in material testing techniques for both analytical models and experimental procedures. Indentation has proven itself to be an invaluable material testing tool for many years. Recent improvements in the accuracy of indentation testing technology have proven

indentation as an accurate means of determining the material properties of homogeneous thin film coatings for films as thin an 1μm (T. Chudoba, 1999). The success of indentation, particularly spherical indentation, in the determination of material properties of homogeneous film coating currently makes it of interest with respect to determining the material properties of nonhomogeneous functionally gradient coatings.

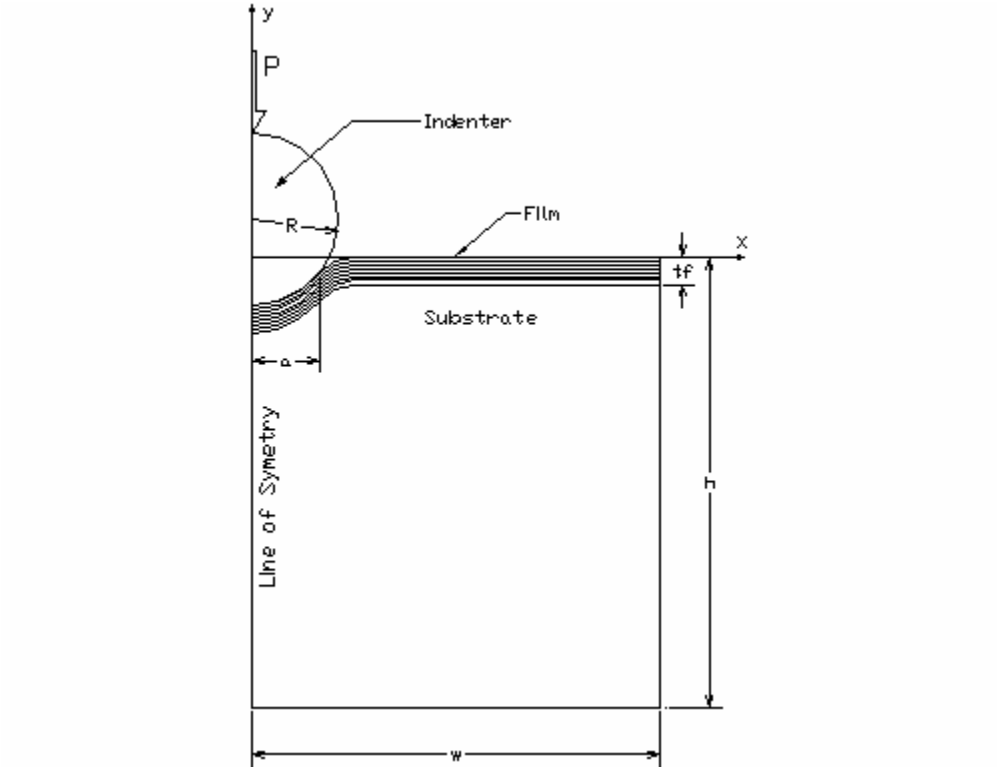

Figure 2: Depiction of spherical indentation on an axisymmetric half space

1.3 Literature survey

A brief overview of the research in this area begins with Chudoba, et al. (2000) who used an analytical solution for the elastic deformation of the substrate to simulate load-displacement data. The model allowed the modulus of thin films

to be determined independently from the effects of the substrate. Later, in 2004, Chudoba et al. (2004) used a theoretical model to derive the correct moduli at the lower and top part of the graded coating. These theoretical models proved to be in agreement with values obtained from experiments.

Chudoba, et al (2002) looked at layered systems and studied interfacial stresses to show effects of adding intermediate layers in improving overall properties of such systems. These results are based on their earlier works (Schwarzer, et al 1999, Schwarzer, 2000) with potential theory. Diaoa and Kandorib (2006) conducted a finite element analysis of the local delamination of a hard coating under sliding contact, and studied the delamination as a function of the relative shear strengths of the coating and substrate, and the ratio of coating thickness to contact width.

Linss et al (2005) used theoretical modeling and nanoindentation testing to investigate the mechanical properties of graded thin films with varying Young's modulus. Their findings showed that through the use of a variety of different spherical indenters that a graded coating could be distinguished from a homogeneous layer.

Several studies have been conducted in the last three decades on the contact and indentation problem of nonhomogeneous materials. Suresh (2001) and Schwarzer (2004) best describe these studies in their review articles. Recently, Ke and Wang (2006) studied the problem of frictionless contact analysis of layered materials with arbitrarily varying elastic moduli.

Advancements in the capabilities of computer modeling and processing have allowed for the use of the finite element method to be employed in the modeling of material coatings and spherical indentation. Additionally, the development of finite element analysis (FEA) programs such as ANSYS 10 assists in the use of this method.

Early studies using FEA in indentation modeling were conducted by K. Sadeghipour (1994), who modeled cracks propagating in polymeric materials subjected to indentation. Sadeghipour (1994) ran extensive simulations to determine specimen geometry and boundary contentions suitable for modeling both the specimen and the indenter in spherical indentation. Many of the modeling techniques used in our study were, in fact, based on the results from this portion of his study.

X. Cai (1995) used the finite element method to simulate the indentation process of a wedge-shaped indenter into Al/Si and TiN/HSS film and substrate systems. Specimens were built up by a 3μm thin coating, a semi-infinite substrate, and a 0.1 μm interlayer. From the results of this study, X. Cai (1995) was able to investigate the indentation load vs. indentation displacement relationship and the influence of the interface on hardness measurements and determined interface's effects on hardness measure was negligible.

Chalasani et. al (2006) developed theoretical models of layered film and substrate configurations modeled as both a nonhomogeneous or homogeneous layer. Their study focused on load-displacement profiles, contact pressures, and critical stresses that can lead to debonding in some film and substrate

configurations. By comparing contact depth and critical interface stresses, the effects of indentation area, film and substrate models, and Young's Modulus ranging from 1:1 to 200:1 were investigated for nonhomogeneous and homogeneous film configurations. Chalasani modeled the indenter load on the surface as a Hertzian stress boundary condition as opposed to a mixed boundary value problem. His findings suggested that critical stresses in these two models varied as much as 15% between the nonhomogeneous and the homogeneous models for Young's modulus ratios greater than 25:1.

1.4 Current study

This study uses finite element analysis (FEA) to investigate the relationship between homogeneous and nonhomogeneous film and substrate geometries subjected to spherical indentation. This study focuses on three relationships determined through a series of FEA simulations conducted on variety of coating models.

First, we investigate the validity of the use of a displacement boundary condition by applying a known force from which a maximum displacement is determined in the simulation. Then, this displacement is reapplied and the resulting critical stresses between the two models are compared.

Second, we investigate the effects of modeling the film coating as either a functionally gradient material with linearly varying material properties or a homogeneous layer in which the material properties are determined by taking an average of the material properties of the substrate and the film surface. Critical

normal stresses, shear stresses, and maximum indentation depths from these models are compared and the force required to create the indentation depth is determined.

Third, regression models are developed from the results of the FEA models and a coefficient from regression is found from each of the nonhomogeneous and homogeneous indentation models at each contact length from the previous simulations. These results are then compared to the Hertzian contact models by developing a pressure field based on the force determined in the displacement boundary condition simulations. The R^2 values from the regression models and the relationship between the force-based coefficient and the regression based coefficient are compared to assess the validity of the Hertzian contact assumption for both the layered nonhomogeneous and the homogeneous modeling techniques.

Chapter 2: FEA Modeling

2.1 Introduction

ANSYS 10 was used for the finite element simulations conducted in this study. The software was chosen for its ability to solve complex nonlinear problems as well as its ability to employ gap elements for contact problems. Additionally, ANSYS load step/substep control made the software capable of retrieving data that occurred at various points along the contact depth as the displacement of the indenter was depressed. This allowed for several contact length to film thickness ratios to be determined in a single simulation given a high enough number of substeps.

An axisymmetric half space of the indentation model was developed for the finite element simulation in order to minimize computational time. The symmetric nature of the stresses that occur in the spherical indentation process along with ANSYS's ability to simulate this type analysis for a wide variety of elements allow for this assumption. A similar study conducted for a spherical indentation modeling and using the same contact elements and axisymmetric assumption reported a 0.1% deviation from the Hertzian theory (ANSYS) which is known to be exact for a homogeneous half space (Schwarzer, 2004).

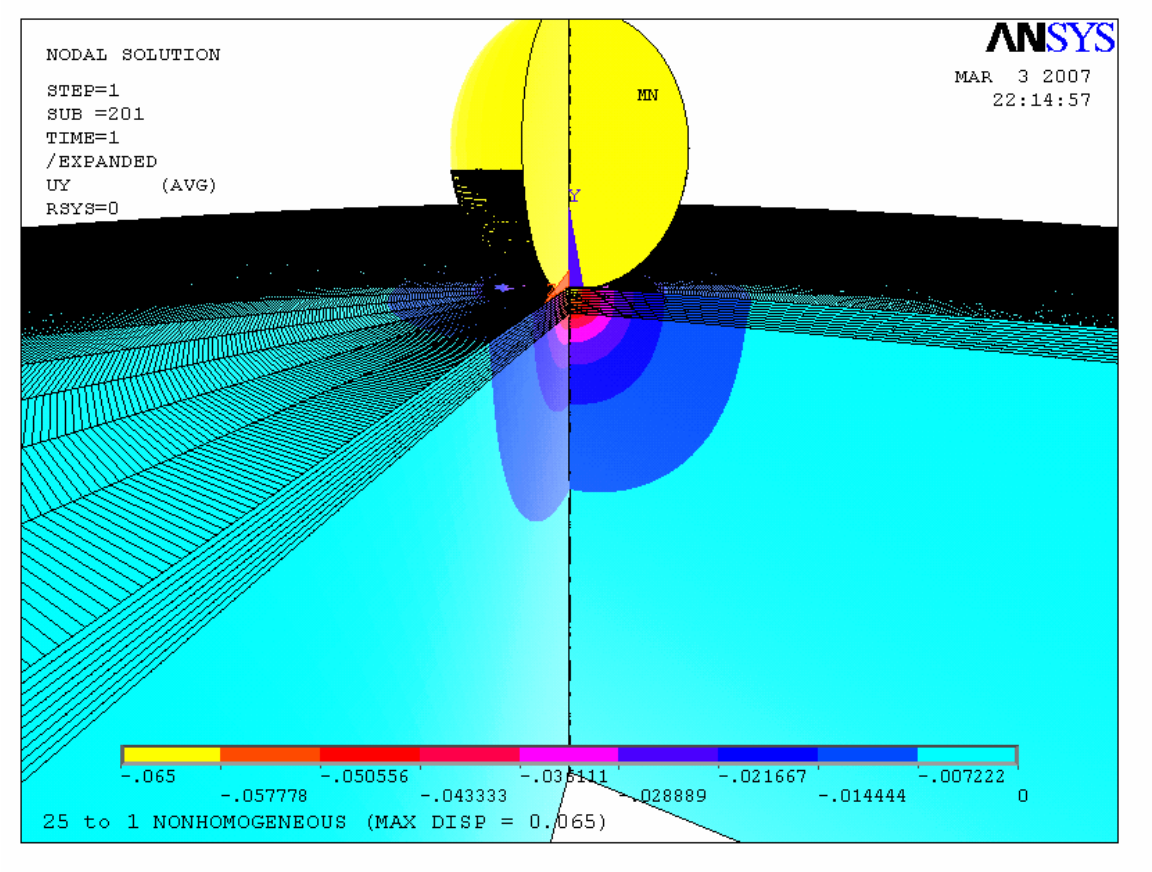

Figure 3: ¾ expansion of the axisymmetric FEA model generated by ANSYS

2.2 Modeling the film and the substrate

The development of the FEA simulation required that all dimensions used in model be both discrete and based on aspect ratios or geometry that fall within the realm of techniques currently used in the spherical indentation process and with geometries that allowed for accurate modeling by finite element analysis. An appropriate height of the model was necessary to minimize the influence of the substrate thickness on the stress results in the film layer(s). The ideal model would be one that had an infinitely thick substrate and discrete thickness for the film layers. This being the case, it was necessary to determine a substrate thickness that was both of a discrete value and thick enough to minimize the effects of the boundary conditions in the stress results that occurred in the area localized about the interfaces of the layers and on the surface contact area. In a study dealing with spherical indentation that used a similar modeling approach and boundary conditions, Sadeghipour (1994) found, after extensive simulations, that a relatively thick model, one where the ratio of the radius of the indenter, R, and the overall height of the specimen, H, was 1/12 (R/H=1/12) satisfied these conditions for elastic stress modeling. This aspect ratio was used for all height and width geometries in the simulations conducted in this study.

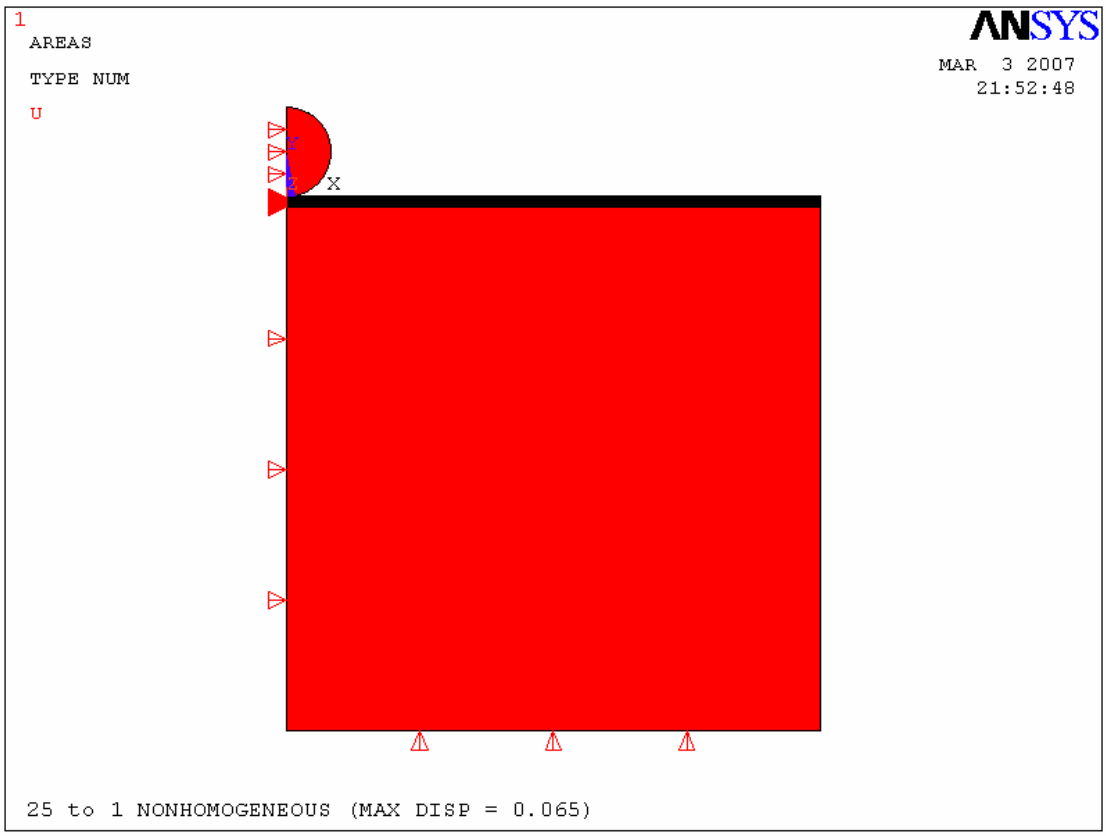

Figure 4: Full view of the FEA model in ANSYS depicting the indenter, the film layers, the substrate, and the boundary conditions

A single film and substrate model was used for all simulations, however, material properties within this model were changed to represent modulus ratios as well as the nonlinear and homogeneous coating properties. To model the coating as a nonhomogeneous material, the film was broken up into ten sub layers that were assigned different material properties. Because the focus of this study was to examine the effects of modulus ratios, the Poisson's ratios for both the substrate and the coating were kept at 0.3 for all simulations and configurations.

To represent the coating as a nonhomogeneous material, moduli values were assigned to each layer and distributed by linear variation with the highest modulus value, E_1, on the coating surface at y=0 to the lowest modulus value of E_2 which equaled that of the substrate at the lower surface of the coating $y=T_f$. A function was developed from each case to represent the linear variation of the moduli. This model was a simple straight line modeled by the function:

$$E(y) = \frac{(E_1 - E_2)}{T_f} y + E_2 \qquad (1)$$

where

$E(y)$ is the value of the Young's modulus at a vertical depth

and y is the vertical depth.

Because each material layer was required to have a discrete modulus value, it was then necessary to determine the average modulus value between the upper and lower portions of each layer. To determine this, the average modulus value, E_i, in each layer was calculated using:

$$E_i = \frac{\int_{h_i}^{h_{i+1}} E(y)dy}{h_{i+1} - h_i} \quad (2)$$

where

h_{i+1} is the vertical depth in the *y*-direction of the upper surface of the layer and h_i is the vertical depth in the *y*-direction of the lower surface of the layer.

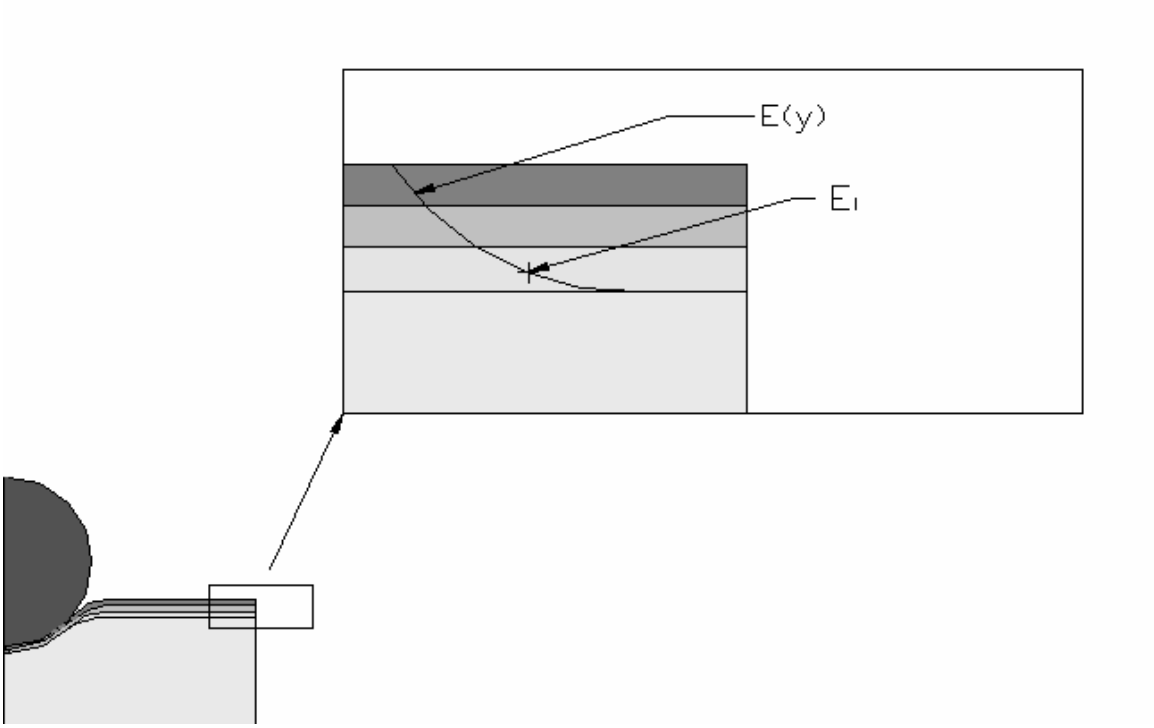

Figure 5: Representation of the material property distribution used in the layered nonhomogeneous simulations

2.3 Modeling the indenter

Indenter radius was based on aspect ratios to film thickness and was initially altered in the design of the FEA model to produce various contact length to film ratios. Film thickness was, however, maintained to be one-half unit thick and subdivided into multiple layers of varying material properties. The overall height and the width of the model were then parametrically based on the indenter radius and altered to determine the correct indenter radius during the modeling phase. In the end, an indenter radius of 2 units was chosen because, it provided the broadest range of acceptable contact length to film thickness ratios that could be achieved for the modulus ratios used in this study.

2.4 Boundary conditions

The boundary conditions used in the FEA model were based both on the axisymmetric assumption and loading conditions imposed in the simulation. Boundary conditions were based on those used in an axisymmetric FEA study conducted by Sadeghipour (1994) for spherical indentation. Due to the symmetric nature of stresses that evolve about the vertical axis in a body subjected to spherical indentation an axisymmetric half space model was acceptable for the purpose of simulation. This assumption required that displacements about the vertical axis at the line of symmetry for both the indenter and the film and substrate model be constrained from movement in the horizontal direction. The base of the specimen was fixed along its entire length in the horizontal direction (*x*-direction) from any displacement that might occur in the vertical direction (y-direction). Movement of the indenter in the *y*-direction was given a fixed negative value by the boundary conditions for displacement loading. Figure 6 shows a graphical view of the boundary conditions.

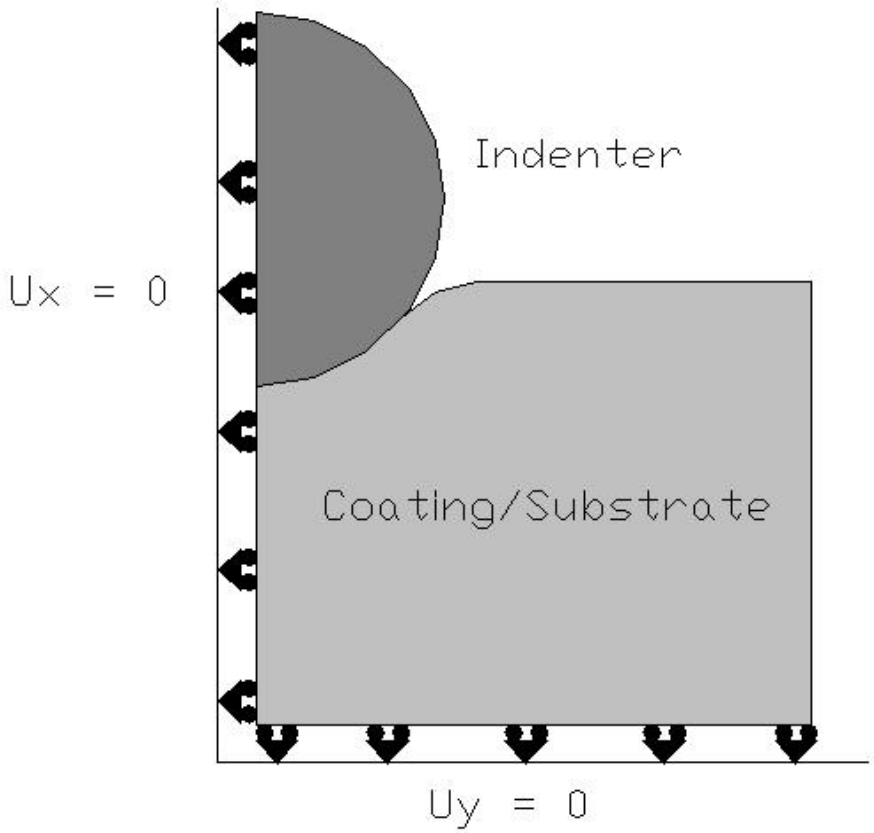

Figure 6: Graphical representation of the boundary conditions used in the FEA model

2.5 Meshing the model

After the basic geometry of the model was created in the software, it was necessary to determine the proper mesh for the indenter, the sub layers, and the substrate. Due to the contact that occurred between the layers, the interface between film layers, the film and the substrate, and the contact between the indenter and the film surface, it was also important that contact (gap) elements be used at the lines that occurred in these regions. Because the model was based on an axisymmetric assumption and developed in two dimensions, planar elements for the areas and contact elements for the lines were used. For all areas occurring in the layers, the substrate, and the indenter, the planar element PLANAR182 was used. The lines between upper contact surfaces were meshed as CONTA171 and the lower target surfaces in the contact surface were meshed as TARGA169.

PLANE182 was used for all area in the simulations including the indenter, the film layers, and the substrate. PLANE182 is a 2-D element used for modeling solid structures. The element was chosen because it has a KEYOPT for use in axisymmetric modeling and it can be coupled with CONTA171 and TARGE169 elements to define contact and target pair relationships. Additionally, PLANE182 is capable of being used in cases of large deflection and large strain. The element is defined by four nodes, each of which has two degrees of freedom for translation in the *x* and the *y* directions. The element also has the capability to be used for plasticity, hyperelastic, stress stiffness, large deflection, and large strain.

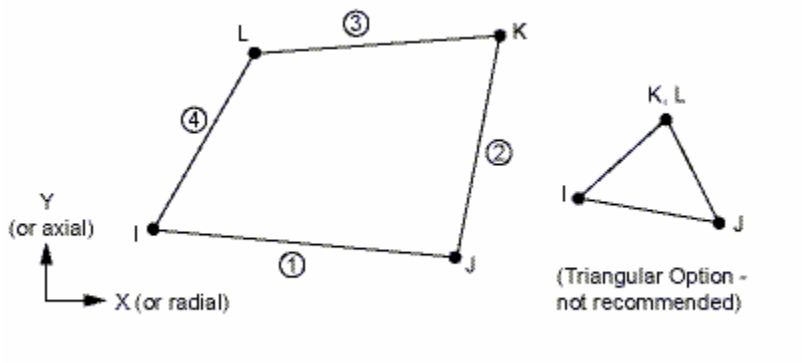

Figure 7: Structure of the PLANE182 element (ANSYS)

The element CONTA171 is used to represent contact and sliding between two surfaces in a contact/target pair for 2-D structural and coupled field analysis. The contact between this element and the target surface occurs when the element surface penetrates one of the target surface elements. The relationship between a contact and a target pair in ANSYS is accomplished by fixing a set of REAL constants between the contact elements and the target elements and meshing the pair along lines or elements designated in the mesh attributes in preprocessing. For this reason, it was necessary with our model to define a total of 12 contact and target pairs to represent the indenter's contact with the target surface of the coating at y=0 and the contact/target relationships that occurred between the film layers and the last film layer with the substrate.

An accurate representation of the element's behavior in the indentation model required that the KEYOPTs and the REAL constants for each of the contact and target pairs be defined appropriately. The most crucial parameters used in this element were those that described the friction that occurred between

the indenter and the film surface and those that defined the element behavior at the interfaces.

In our simulations, the friction between the indenter and the film were designated to be zero in all models. The reasoning for this is that the effects of friction between the indenter and the film surface vary between materials and ultimately should be minimized or cancelled out in the stress ratios between these two models.

For the interfaces between the film layers and the interface between the film and the substrate, the CONTA171 parameter for sliding was fixed so that nodes on the upper layer of the interface (TARGE169) and the lower layer of the interface (CONTA171) were fully bonded and constrained from any delamination and sliding that may occur. Additionally, fixing the layers together ensured continuity of displacement between the film layers. Vanimisetti (2005) also used this constraint in the ABAQUS/Standard software for the purposes of modeling the interface between film layers.

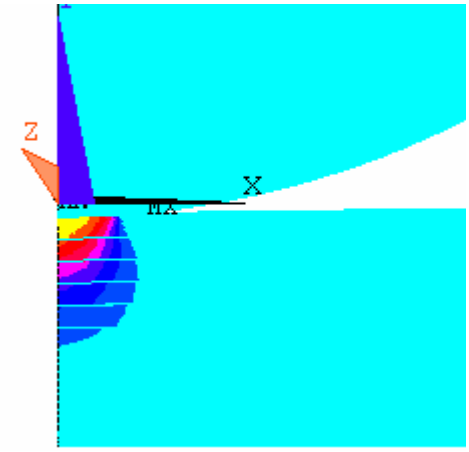

Figure 8: Contour plot showing the stress continuity in σ_{yy} for a layered nonhomogeneous model

A full description of the CONTA171 KEYOPTS and REAL constants used in the FEA model are listed in Table 1: Relevant KEYOPTS for the CONTA171 elements.

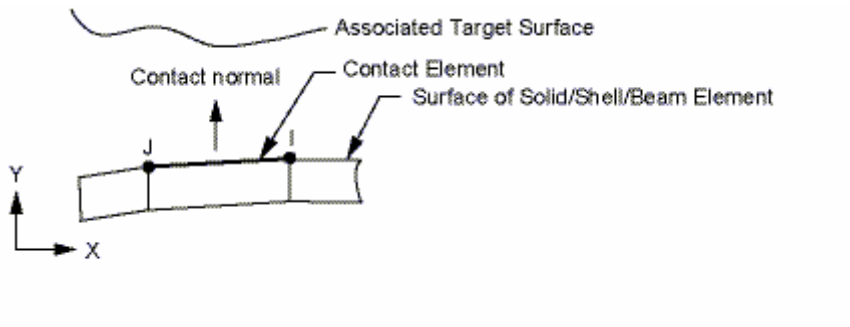

Figure 9: Structure of the CONTA171 element (ANSYS)

Target elements describe the boundary of a deformable body that is potentially in contact with a surface element. The element TARGE169 corresponds with the use of the element type CONTA171 for contact and target

pairs. TARGE169 was used for all upper surfaces of the film layers and the upper layer of the substrate in the FEA model. The majority of KEYOPTS and REAL constants of interest in the contact and target pair were fixed by the CONTA171 KEYOPTS and REAL constants. ANSYS describes the element TARGE169 as the associated target element for the contact elements CONTA171, CONTA172, and CONTA175.

A useful trait of the target element TARGE169 is that forces and moments can be imposed on this surface independent of a contact element. For this reason, the pressure displacement models used in the simulation did not require that the model be reconfigured for analysis. It only required that the corresponding pressures be imposed and the displacement of the indenter in this case be fixed to zero for all degrees of freedom.

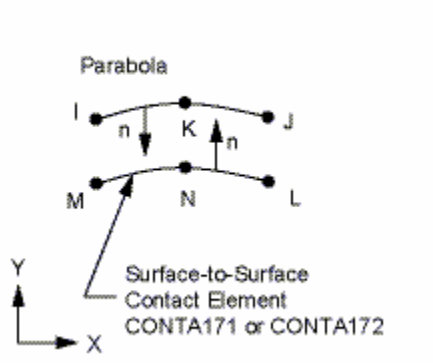

Figure 10: Structure of the TARGE169 element (ANSYS)

2.6 Overview

The following table provides an overview of the KEYOPTS used in the simulation and the portion of the model to which they correspond. With the exception of the film layer in direct contact with the indenter, the KEYOPTS and real constants of the contact and target pairs were consistent with each other, although defined separately for each surface. For this reason, the following table only needed to be defined in two sections to represent all of the KEYOPTS used in the contact and target pairs in the simulation.

Table 1: Relevant KEYOPTS for the CONTA171 elements

CONTA171: Lower film layers

KEYOPT	*Description*	*Status*	*Status Description*
1	Selects degrees of freedom	0	UX,UY
2	Contact Algorithm	0	Augmented Lagrangian
3	Stress state when superelements are present	0	NA/Default
4	Location of contact detection point	0	On Gauss point
5	CNOF/ICONT automated adjustment	4	Auto ICONT
12	Behavior of contact surface	5	Bonded (Always)

CONTA171: On the indenter surface

KEYOPT	*Description*	*Status*	*Status Description*
1	Selects degrees of freedom	0	UX,UY
2	Contact Algorithm	0	Augmented Lagrangian
3	Stress state when superelements are present	0	NA/Default
4	Location of contact detection point	0	On Gauss point
5	CNOF/ICONT automated adjustment	4	Auto ICONT
12	Behavior of contact surface	0	Standard (Frictionless)

Chapter 3: Model Verification

3.1 Introduction

It was determined early on in the development of the FEA model that the proper mesh size and element choice would play a vital role in accurately modeling the indention process. A coarser mesh at the lines of contact was found to produce stresses in a fully homogeneous half space model that were both inconsistent and incorrect when compared to the exact solution from the theoretical Hertzian contact model. For this reason, model verification assisted not only with the evaluation of the correctness of the model, but also with the overall development of refinements and element choice that were used. Model verification of the FEA model used in this study consisted of three procedures that will be fully outlined in this chapter. These procedures included:

1.) Comparison to Hertzian theory for axisymmetic geometries when the model was defined as a fully homogeneous half-space.
2.) A convergence study for the lowest modulus ratio (1:1) and the highest modulus ratio (200:1).
3.) An assessment of stress continuity at the interfaces between the film layers.

The model verification process took place each time that the FEA model changed in geometry and loading configuration.

The limited nature of the educational version of ANSYS 10 for educational purposes required that a maximum of nodes be defined in the model. Although the maximum number of nodes was beyond that necessary for the 2-D axisymetric half-space model, due to the heavy usage of contact and target elements, it was determined through several attempts to be too low for 3-D modeling in this study.

3.2 Comparison to Hertizan results

When the mesh in an FEA model that is correctly defined is refined, the overall error in the solution should reduce, however, the computation time for the solution increases greatly with the number of nodes present in the model. Additionally, the limitations of the software provide an upper limit to the number of nodes that can be defined in a body. For these reasons, mesh refinements at areas of importance with respect to the final solution as well as to the conditions defined in the loading can often be useful in limiting the processing time without incurring great losses in the solution's accuracy. In our case, the portions of the model determined to be of the greatest importance and thus requiring the heaviest refinements were the contact portion on the indenter, the contact portion of the film surface, and the contact portions of the individual film layers where the maximum normal stresses, shear stresses, and displacements occurred.

Early models created using a coarser mesh (element length greater than $1/48^{th}$ of the specimen width) were found to produce such stress results when compared to Hertzian theory that to list the results would be irrelevant. The reason for this was probably the error incurred in the simulation between the contact elements and the target elements in the region of the contact area. When meshed coarsely, elements viewed in a displacement plot in the postprocessing phase of the simulation, appeared to pass through each other rather than to induce contact between the specimens. For this reason, the mesh in the extending past the contact area (from x=0 to x=1) was refined at the surface. The mesh was also refined to a depth just past the last film layer into the substrate and refined along the lines between the film layers and the last film layer to the substrate. The original guidelines for these refinements came from those used by Vanimisetti (2005) for modeling film and substrate configurations using FEA, however, refinements along the interface between the last film layer and the substrate were more heavily refined in our study due to the interest in the shear stresses in this region. These refinements alone greatly improved the results, however, it was necessary at this point to determine how much refinement was necessary.

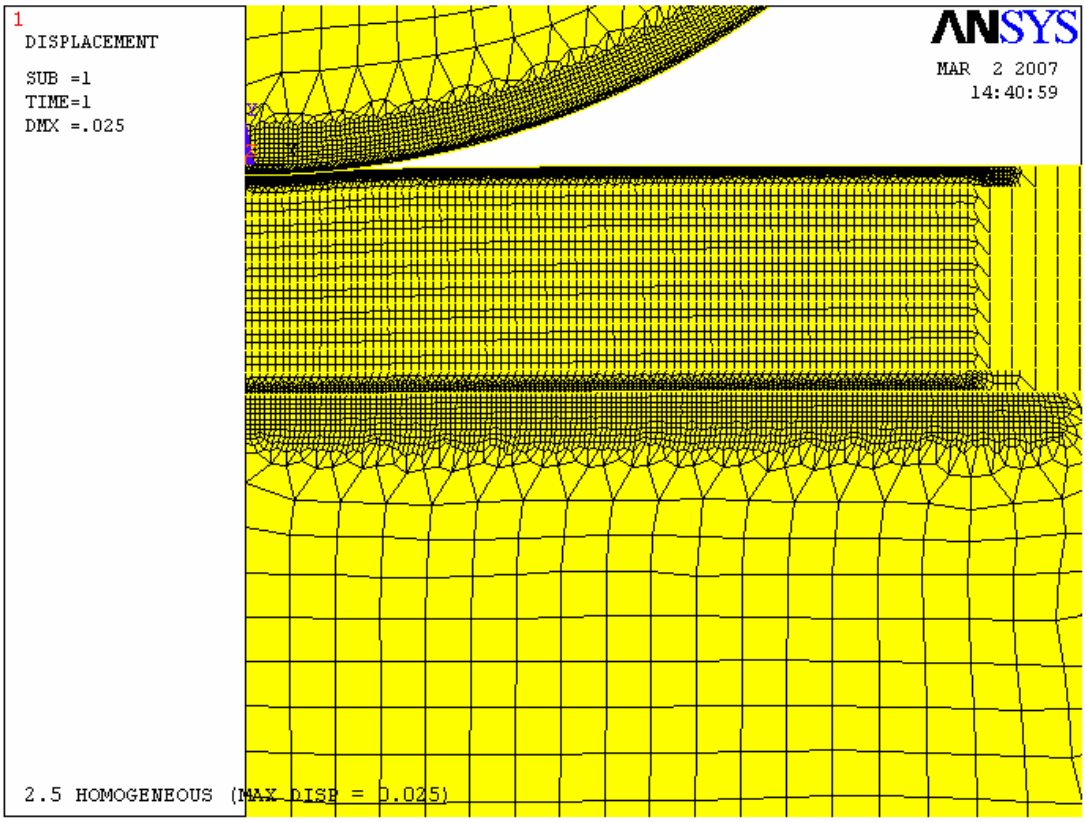

Figure 11: Mesh refinements

The initial determination of the mesh refinement requirements was an iterative process that involved the following steps:

1.) Defining a course mesh and evaluating the region of contact irrespective of the error in the magnitude of the stresses,

2.) Refining the portions of the previous model and then running the simulation,

3.) Comparing these results to the Hertzian model to determine whether or not additional refinements were necessary.

When the error of the FEA model in comparison the Hertzian model was less than 5% for the maximum normal stress at the surface, σ_{yy}, it was necessary to conduct a convergence study on the current mesh to determine whether or not further refinements would reduce error.

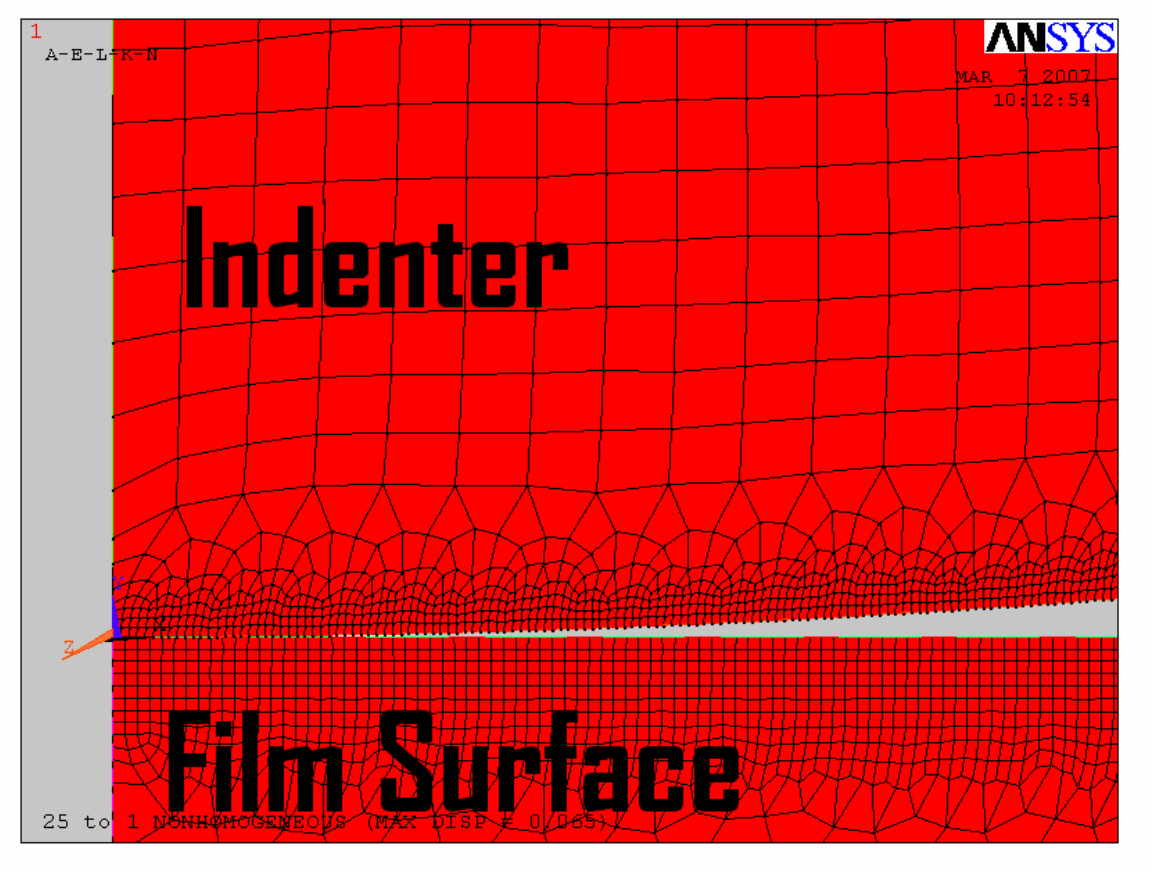

Figure 12: Contact between the indenter and the film surface

3.3 Convergence study

Convergence testing on an FEA model calculates discretization errors by evaluating the results from the model at several levels of mesh refinement. It also can, in some cases, help to determine whether or not a singularity occurs in the model. Using a single geometric model with fixed material properties and geometry, several levels of refinement are brought onto the mesh and the simulation is run for each of these levels of refinements. Data at a given point in the model was collected for each of the levels of refinement and a convergence test was conducted using the mathematical model.

Let R_N be the resulting output using N number of elements, then A is the result using an infinite number of elements in

$$R_N = A + \frac{B}{(N)^{\alpha}} \tag{3}$$

where

B is a constant and,

α is the rate of convergence.

From equation 3 it can be seen that as N approaches infinity that the value of R_N, which represents a theoretical value of the result, with an infinite mesh, becomes A if the term α is greater than 1. Also note that there are three unknowns (A, B, and α) showing that results from three meshes must be used for this convergence test to be conducted.

A sample convergence test of the mesh that was used in this study produced the following results:

Table 2: Results from sample convergence test

N	A
20	-383.76
30	-395.78
40	-397.76

which resulted in the equations

$$\sigma_{yy1} = -383.76 = A + \frac{B}{20^{\alpha}}$$
$$\sigma_{yy2} = -395.78 = A + \frac{B}{30^{\alpha}}$$
$$\sigma_{yy3} = -397.76 = A + \frac{B}{40^{\alpha}}$$

Solving these three simultaneous equations, the following results were found

$$A = -398.655$$
$$B = 2.828 \times 10^{6}$$
$$\alpha = 4.057$$

which showed that the theoretical value of the stress at this point *A* was equal to -398.655 and that α>1, indicating that the results will converge and that there was a decrease in relative error resulting from the refinement of the mesh.

3.4 Continuity checks

After evaluating the results from the mesh by comparison to the Hertzian model and developing an adequate mesh as found by convergence testing, the model was arranged in the nonhomogeneous form and the continuity of the

shear stresses and displacements was compared at the top and the bottom interfaces of the last film layer to determine whether or not there was a continuous transfer of stresses and displacement across the contact and the target elements. Due to the nature of the mesh, some error was inevitable given the placement of the nodes along the contact surface because node locations at the top and node locations at the bottom of the interface did not necessarily have the same coordinates. The node locations, however, were close enough for comparative purposes (less that $1/10^{th}$ of a element length in most cases) to make a comparison. The final configuration of the model showed continuity across the interface for both stresses and displacements with errors were less than 0.5% for both displacements and shear stresses.

Chapter 4: Simulation of the Indentation Process

4.1 The displacement boundary condition

To simulate a displacement from an indenter onto the surface of the film, the base of the film and substrate model, the line of symmetry of the indenter, and the line of symmetry of the film and substrate were fixed according to the boundary conditions and the indenter itself was given a fixed downward maximum displacement in the vertical direction in the ANSYS software. As the indenter passed through various points along the path to the maximum displacement, data was collected at every substep, or vertical position, along its path. By doing this, it was possible to collect data at a variety of points and correlate the position of the indenter to the contact length to film thickness ratios of interest along the path.

The contact length of the indentation is defined as the length from the first point of contact of the indenter to the last point on the indenter surface that direct contact with the indented specimen occurs. Generally, a contact length to film thickness ratio ranging from 0.2 to 0.4 is considered suitable from measure of material properties from spherical indentation (Chalasani, 2006). Indentation profiles for displacement resulting from spherical indentation at the surface of the indented specimen generally are parabolic in nature and dependent on the material properties of the indented material. For this reason, it is difficult to

assume a contact length based solely on the radius of the indenter and the displacement or force that is applied to it.

The technique used in this study to overcome this challenge was to overshoot the indention depth necessary to produce the contact length to film thickness ratio, a/T_f, and to examine the data that was produced along the path of the indenter to find the displacements that resulted in the correct ratios based the reaction forces that occurred on the film surface as the indenter penetrated the film. From this data, it was then possible to narrow down the depths of interest and to identify a maximum indentation depth that could be used in the final simulations. This procedure reduced the overall processing time by providing more accurate data through a decrease in the number of substeps necessary in the final simulations.

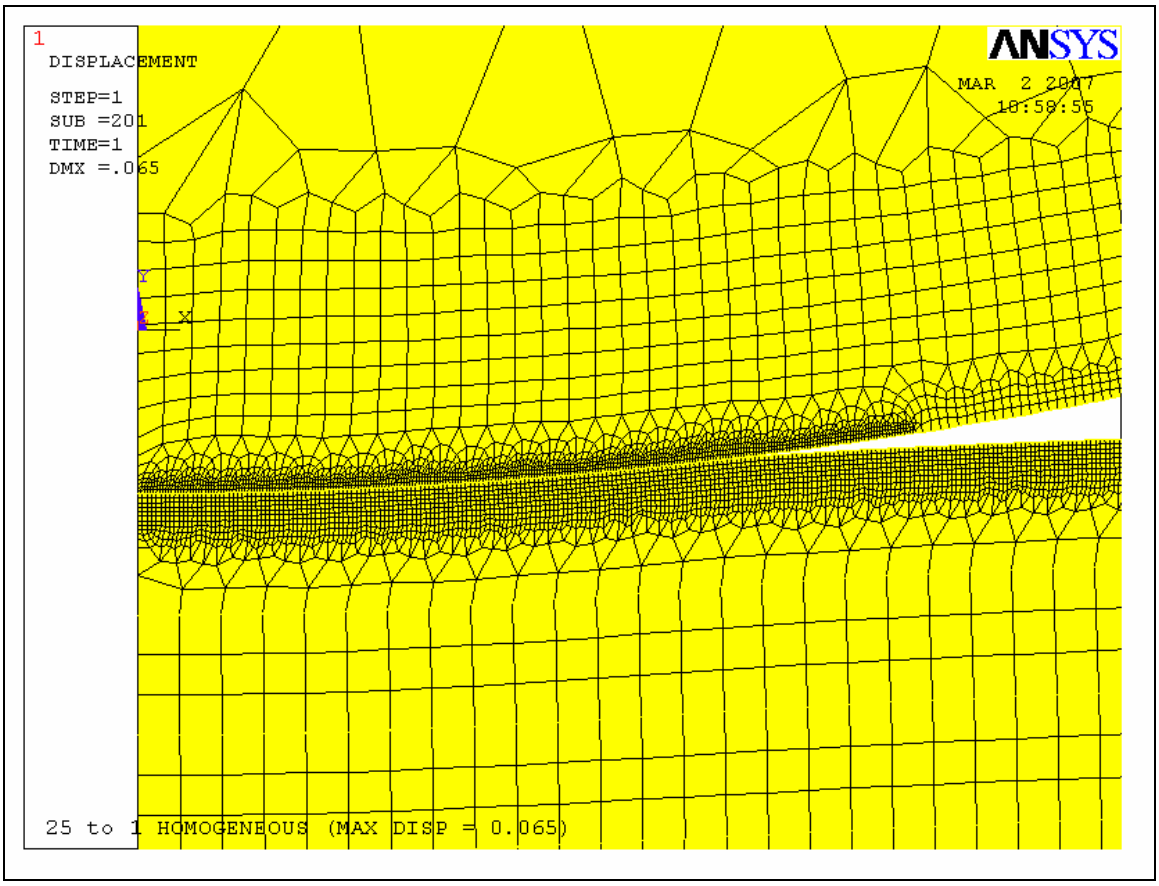

Figure 13: Displacement plot depicting the contact between the indenter and the film surface

4.2 Application of the pressure boundary condition

The pressure models used in this study were developed based on regression models from the data collected in the displacement simulations. The basis for the creation of these models was to determine if a regression model based on the Hertzian contact assumption and calculated through the data that resulting from the FEA simulations would produce a coefficient of similar magnitude to that of the force-based coefficient used in the Hertzian contact model for spherical indentation. The development of these two coefficients from

models independent of each other allowed for the comparison of the FEA nonhomogeneous and homogeneous model data for film and substrate models to the theoretical Hertzian contact model used for fully homogeneous (film and substrate having the same material properties) spherical indentation modeling.

To describe the procedural basis of the development of the coefficients, it is first necessary to examine the pressure field as it is modeled by the Hertzian contact assumption. For a spherical indentation study of an axisymmetric homogeneous half space, the known exact technique for modeling a pressure field is given by the equation:

$$p(r) = \frac{3P}{2\pi a^3}\sqrt{a^2 - r^2} \tag{4}$$

where

P is the force applied to the indenter

a is the contact length, and

r is a point along the contact length

Examination of equation 4 shows that the constant terms can be collected and rewritten as :

$$C_H = \frac{3P}{2\pi a^3} \tag{5}$$

for a given contact depth, ***a***, and equation 5 can be rewritten as:

$$p(r) = C_H \sqrt{a^2 - r^2} \tag{6}$$

where the term C_H represents what will be referred to as the force-based coefficient term.

To determine the force-based coefficient term from the data collected through the FEA simulations, data for the normal stress along the surface in the region of the contact length, a, was collected and then integrated accordingly to determine the force by first creating a cubic spline of the data and then integrating the spline to determine the applied force, *P*, using:

$$P = 2\pi \int_0^a \sigma_{yy}(x)\, x \quad dx \tag{7}$$

Finally, combining the force, *P*, and the remaining terms in C_H, the force-based coefficient term can be rewritten as:

$$C_H = \frac{3}{a^3}\int_0^a \sigma_{yy}(x)\, x \quad dx \tag{8}$$

The derivation of the regression based coefficient began with the pressure field, *p(r)*. Assuming that the stresses in the FEA model for the functionally gradient material followed the Hertzian contact assumption, it follows that, at the surface:

$$\sigma_{yy}(r) = C_R\sqrt{a^2 - r^2} \tag{9}$$

where

C_R is a coefficient determined through regression.

From equation 8, the sum of the square residuals is then:

$$S_r = \sum_{i=1}^{n}\left(\sigma_i - C_R\sqrt{a^2 - r_i}\right)^2 \tag{10}$$

Minimizing the sum of the square residuals by taking the first partial derivative of S_R with respect to C_R then gives:

$$\frac{dS_r}{dC_R} = \sum_{i=1}^{n} 2\left(\sigma_i - C_R\sqrt{a^2 - r_i}\right)\left(-\sqrt{a^2 - r_i}\right) = 0 \tag{11}$$

Whose solution defines the regression based coefficient as:

$$C_R = \frac{\sum_{i=1}^{n} \sigma_i \sqrt{a^2 - r_i^2}}{\sum_{i=1}^{n} (a^2 - r_i^2)} \tag{12}$$

Once the coefficients were developed, the reapplication of the regression coefficient based pressure field to the model from which the coefficient developed was conducted to ensure the accuracy of the regression technique as well as to examine the justification for the use of this technique in modeling. The reapplication of the pressure field in ANSYS required that the pressure be distributed over the contact area after which the simulation was solved so that the results could be compared.

Because the pressure field from the regression model was defined at points along the radius of the contact length, it was necessary to then determine the value of pressure across individual element length in the FEA model to

reapply them in ANSYS. To accomplish this, the trapezoidal rule was used between the pressure values at individual nodal locations and the pressure determined by this procedure was applied to the element surface between these nodes. The pressure between two consecutive nodes using this method was defined by the trapezoidal rule as:

$$p_i = \frac{\int_{x_i}^{x_{i+1}} \sigma_{yy}\, 2\pi x \quad dx}{\pi(x_{i+1}{}^2 - x_i{}^2)} \tag{13}$$

where p_i is the pressure applied to the element surface

x_i is the x-location of the first nodal pressure

x_{i+1} is the x-location of the second nodal pressure

The first pressure applied from equation 12 was defined across the first element along the line of symmetry. As a result of the method used to distribute the pressure across the contact length, it was not possible to apply a pressure at the last element in the contact length, however, the nodal spacing was created using a very fine mesh and the pressure at this location was significantly low as have a negligible influence over the results.

4.3 Load step and substep procedures

All simulations required ANSYS to perform nonlinear analysis in the solution phase. Solution controls were set to large displacement static mode. A range of substeps which varied from simulation to simulation were used to produce the final results, but the maximum number of substeps ultimately used in the solutions were determined by the ANSYS solver using a modified bisection method. The solution method that was fixed by the PLANE182 element was modified Lagrangian. CONTA171 KEYOPT for AUTO ICONT corrected the initial penetration gap by adjustments in the first substep. Results at every substep were written and saved to the database for postprocessing after the solution completed.

The program for the geometry and the mesh was initially written in the form of an ADPL logfile but was later saved as 15 database (.db) files with varying displacements and material properties that corresponded to each of the modulus ratios for the homogeneous and the nonhomogeneous simulations.

Simulations were run on two computers. The first used a 1.0 GHZ Pentium 4 processor with 1 GB of RAM. The second computer used a 1.0 GHZ Pentium 4 and processor and 512 MB of RAM. Solution times varied by computer and case but generally ran from 3 ½ hours to 5 hours per simulation. Overall, each full batch of simulations took approximately 75 hours of processing time to complete.

Simulations were run to determine the stresses and displacements that occurred at the surface and the interface for homogeneous and

nonhomogeneous-layered models with moduli ranging from 1:1 to 200:1. Each simulation provided data for a/T_f values ranging from 0.2 to 0.4. To retrieve the data at those values, the loading was broken up into a series of substeps and the indenter displacement that produced the correct a/T_f ratios were determined by the following steps:

1.) Stresses at the nodes corresponding to the a/T_f ratio of interest were written to a lister file at each substep after the solution completed and a range of substeps that the correct ratio occurred in was identified.

2.) Reaction forces at the nodes corresponding to the contact lengths that produced a/T_f ratios of 0.2, 0.3, and 0.4 were examined throughout the range of substeps identified in step 1 of this procedure. The substep that produced a positive reaction force was isolated and determined to be the nearest correct substep.

3.) A visual inspection of the displacement plot from ANSYS postprocessor was made to determine if the last node in contact from step 2 of this procedure correctly corresponded with the node required for the proper a/T_f ratio.

4.) If the node from step 2 and step 3 of this procedure was +/- 1 node length (element length of 0.001866667) then the data at this substep was read. If not, then the number of substeps was increased and the simulation was run again.

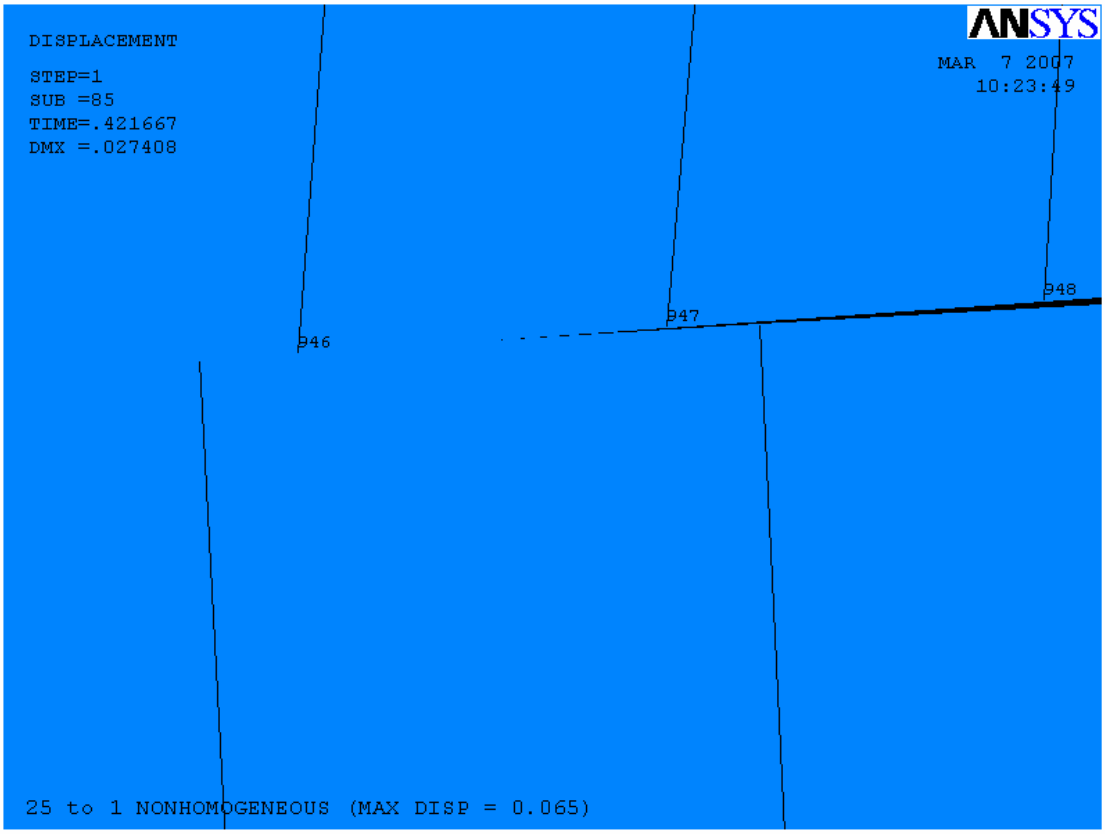

Figure 14: Figure depicting the last node in contact used to define the contact length

Initially, the minimum number of substeps specified for all simulations was fifty. After running all of the cases, it was determined that this number was generally too low for most of the cases, however, the displacements at values of $a/T_f = 0.4$ for all simulations (which represents the maximum displacement that would be required for future simulations) was determined.

By reducing the maximum indenter displacement and increasing the number of substeps through a series of simulations, every time that the simulations were run and step 4 of the procedure above took place, the results became increasingly more accurate. In the end, the majority of the cases required at least 200 substeps to provide accurate results. This being the case, it is interesting to note for future studies that the computation time was not significantly increased by the increase in the number of substeps. Table 2 below shows the number of substeps and the ultimate maximum displacements specified in the final simulations from which data was collected.

Table 2: Substep listing and maximum indenter displacement boundary conditions listed for all simulations

Case	*Min. number of Substeps*	*Max. Indenter Disp*
1:1	200	0.025
2.5:1 H	200	0.025
2.5:1 NH	200	0.025
5:1 H	200	0.035
5:1 NH	200	0.035
12.5:1 H	200	0.045
12.5:1 NH	200	0.045
25:1 H	200	0.065
25:1 NH	200	0.065
50:1 H	200	0.085
50:1 NH	200	0.085
100:1 H	200	0.15
100:1 NH	200	0.15
200:1 H	100	0.2
200:1 NH	100	0.2

4.4 Data post processing

After the substeps corresponding to the correct a/T_f values for each simulation were determined, a program was run in APDL that isolated the nodes at the surface ($y=0$) and at the interface ($y=T_f$). Stress and displacement data at these substeps were written to lister (.lst) files by the ANSYS postprocessor and later exported to Excel for evaluation. At this point, the data was analyzed and critical data points were isolated.

The stress profiles in Excel were imported to MathCAD for the development of the pressure boundary condition coefficients. The ability of MathCAD to easily handle large quantities of data and perform a wide variety of complicated calculations made it more suitable than Excel for the development of

the pressure boundary condition inputs and the comparisons to the Hertzian contact model (that were used in the model verification).

The outputs from the calculations handled by MathCAD were then exported back to an Excel worksheet after which ADPL code was developed for the pressure boundary condition simulations.

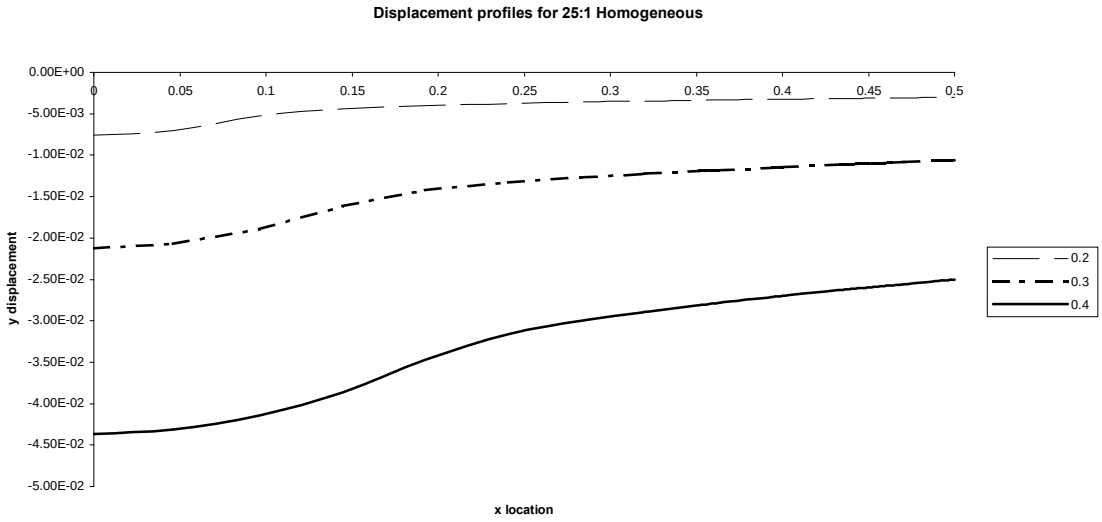

Figure 15: Sample displacement profiles for a/T_f values of 0.2, 0.3, and 0.4

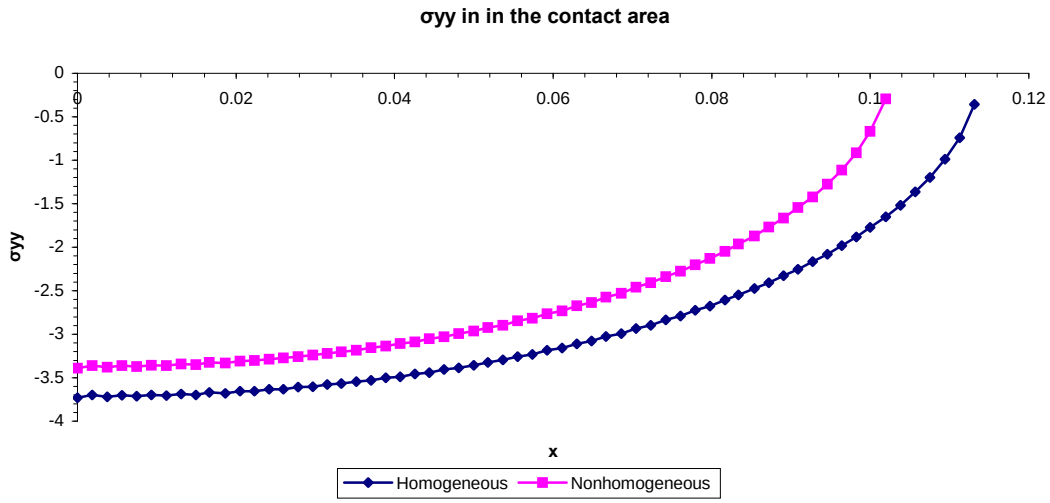

Figure 16: Sample comparison of normal stresses, $\sigma_{yy,}$ along the contact length for homogeneous and nonhomogeneous film models.

Chapter 5: Results and Discussion

5.1 Introduction

Data from the FEA simulations was obtained to indicate contact depth, maximum normal stress at on the film surface, and maximum shear stress at the film to substrate interface for different values of film to substrate Young's modulus ratio, contact length to film thickness ratios, and homogeneous or nonhomogeneous representations of the film layer modulus.

Results are given for both the linear variation model for elastic modulus as well as the homogeneous elastic modulus model. The variations in the FEA model results from these modeling techniques are examined by comparing the ratios of the nonhomogeneous and the homogeneous models as well as through comparisons between coefficient terms derived from either regression or through calculation of the force applied to the indenter.

5.2 Hertzian contact assumption

The validity of the use of a displacement boundary condition was confirmed by first applying a known force to the indenter in the FEA model and collecting this data then, from that data, we apply the resulting maximum displacement of the indenter and compare results. Simulations showed that for every case, the resulting of critical normal stresses, shear stresses at the

interface, and the displacement profile itself did not vary between the two methods.

The accuracy of the FEA model used for the layered cases as well as the correctness of the derivation of the regression coefficient was confirmed by applying a known force to the indenter in a fully homogenous model and comparing the results from this simulation to the known exact results of Hertzian contact theory for an axisymmetric geometry. Based on the results from the 1:1 model, the coefficient from regression was found to have an R^2 value of 0.999. Additionally, when comparing the regression based coefficient and the resulting force-based coefficient used in the Hertzian contact model from this model, the error resulting between the two that was less than 1%.

5.3 Contact depth

Figure 17 depicts the relationship between modulus ratio and contact length to film thickness ratio to the maximum contact depth. The maximum contact depth between the nonhomogeneous and the homogeneous models varied from 14% for the 2.5:1 case to as much as 75% in the 200:1 case. The influence contact length to film thickness ratio effected the variation in the sense that higher a/T_f ratios showed less variation throughout the modulus ratios range than lower a/T_f ratios. The reason for this may be that the effect of the modeling techniques became more pronounced with indentions that penetrated the film layer more heavily.

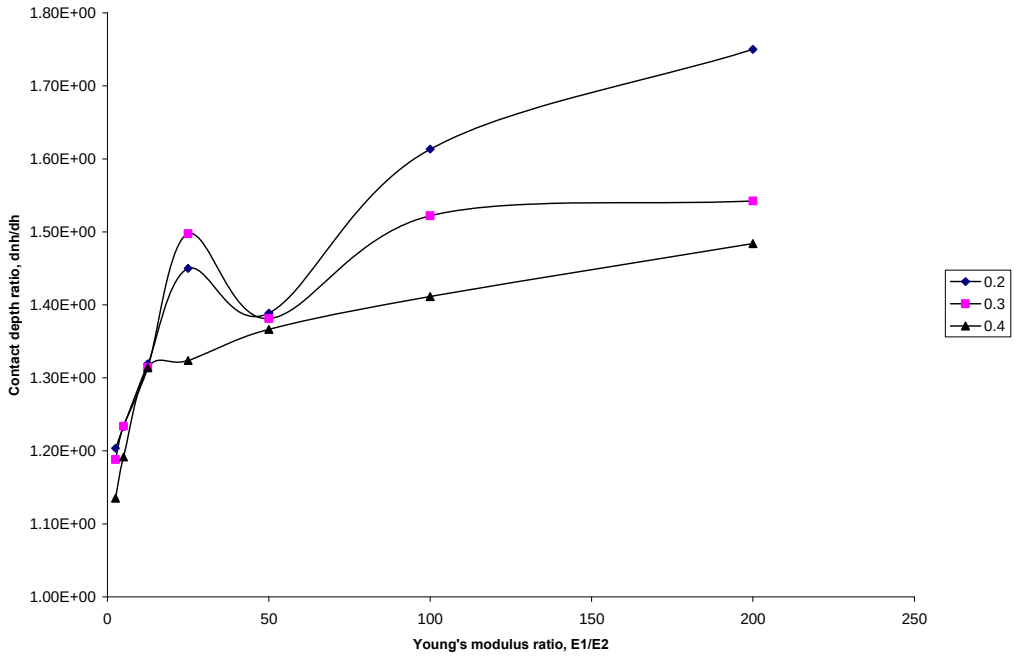

Figure 17: Maximum displacement ratios between the nonhomogeneous and the homogeneous models for Young's modulus ratios ranging from 2.5:1 to 200:1 and a/T_f ratios of 0.2 to 0.4

Note that there is a spreading in the displacement ratios related to a modulus ratio value of 12.5:1. The reason for this deviation in the displacement data in Figure 17 is presumed to be related to the local deviation from the trend of the data in the maximum normal stress at a modulus ratio of 12.5:1 or, conversely, the improvement of the data centered about a modulus ratio of 50:1.

5.4 Maximum normal stress at the film's surface

Figure 18 depicts the relationship between modulus ratio and contact length to film thickness ratio to the maximum normal stress, $\sigma_{yy}^{\max}$, at the surface of the film. The variation in maximum normal stress at the film's surface ranged

from 19% for the 2.5:1 modulus ratio to as much as 66% for the 200:1 modulus ratio. As with the contact depth variation, the influence of the contact length to the film thickness ratio, a/T_f, reduced the variation of the stresses between the nonhomogeneous and the homogeneous models. The reason for this is, again, assumed to be the effect of deeper penetration of the indenter representing an averaged material property in the film vertical cross section.

To validate the planar assumption made by Chalasani (2006), for films of different elastic modulus than the substrate, the film surface was modeled to have a modulus of E_1 and the substrate to have a modulus of E_2 with the intermediate layers following either nonhomogeneous or a homogeneous material properties to represent a transitional interface between a fiber and a matrix. The geometry of the FEA model used in this study allowed for the model and the mesh itself to accomplish this simply with a change in material property throughout the layers. The results of these tests showed that the ratios between the axisymmetric model and a planar case used by Chalasani differ by less than 6% for the maximum interfacial normal stress ratio, 2% for the maximum shear stress ratio, and 4% for the maximum indentation depth showing that the assumption for the planar model was, in fact, valid.

Additionally, it is interesting to note another similarity to Chalasani's work. From the FEA data it appears that maximum normal stress variation appear to have peaked out somewhere around a modulus ratio of 12.5:1 and then dropped down around a modulus ratio of 50:1, and then steadily increase thereafter.

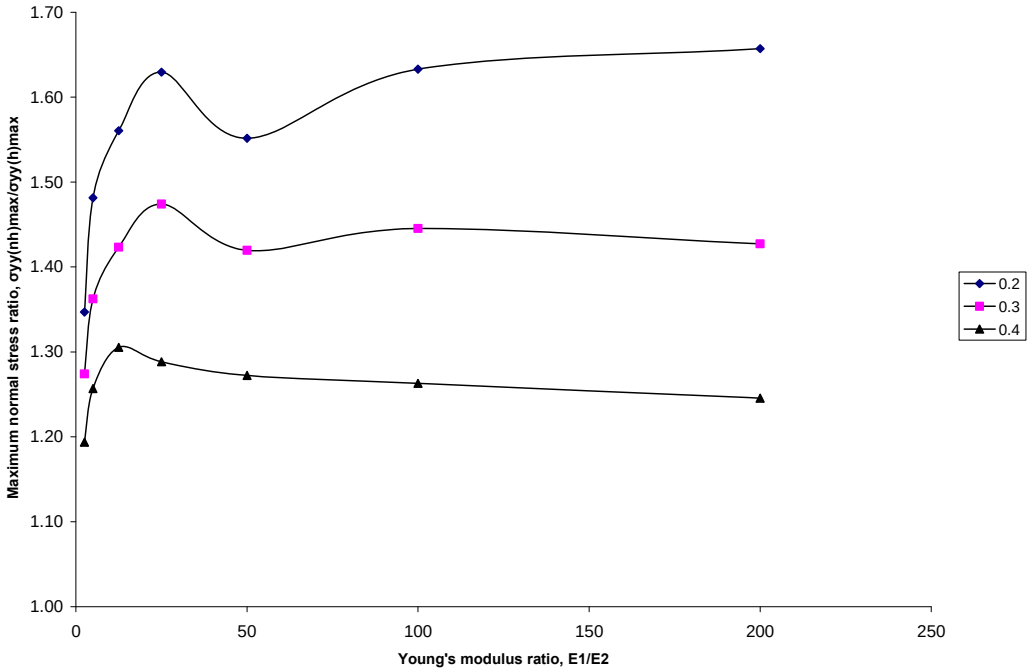

Figure 18: Maximum normal stress ratios between the nonhomogeneous and the homogeneous models for Young's modulus ratios ranging from 2.5:1 to 200:1 and a/T_f ratios of 0.2 to 0.4

5.5 Maximum shear stress at the interface

The difference in the maximum shear stress between the nonhomogeneous and the homogeneous models varied from 19% for a 2.5:1 modulus ratio to 57% for the 200:1 modulus ratio, but reached values as low as 6% for the 50:1 modulus ratio. As with the maximum normal stress data, the ratio appears to have approached a local maximum centered about a modulus ratio of 12.5:1 after which the shear stress ratios briefly decreases but, again, continued to increase as the moduli ratios increased to 200:1.

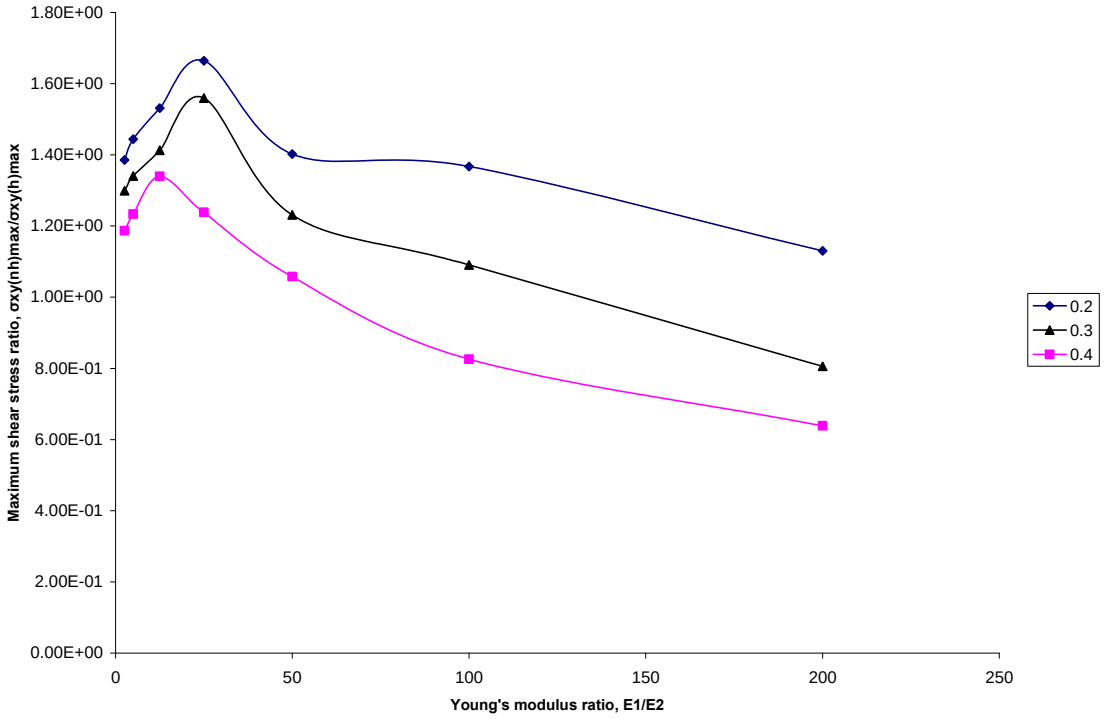

Figure 19: Maximum shear stress ratios between the nonhomogeneous and the homogeneous models for Young's modulus ratios ranging from 2.5:1 to 200:1 and a/T_f ratios of 0.2 to 0.4

5.6 Pressure models and regression models

There was a surprising agreement between the regression based and the pressure based coefficients for both the nonhomogeneous and the homogeneous models as well as the R^2 values for the regression models indicating that both models produced data closely related to the theoretical Hertzian contact model. The explanation for this is that while the nonhomogeneous and the homogeneous material models for the film layer varied greatly when compared to each other from the standpoint of critical stresses and displacements, the overall force applied to the indenter varied accordingly as to be in agreement with Hertzian contact theory. Table 4 shown below lists the

regression and the pressure based coefficients related to a contact length to film thickness ratio of 0.3. Data was chosen at this point because it reflects the average contact range of data collected in the experiment and it is based on a higher number of nodal data points (81) than the data that was collected for a contact length to film thickness ratio of 0.2. This being the case, it should be pointed out that the relationship between the regression based coefficients and the pressure based coefficients listed for an a/T_f ratio of 0.3 in Table 4 were very similar to those from a/T_f ratios of 0.2 and 0.4.

Table 4: Regression based coefficients for a/T_f=0.3 with R^2 values for modulus ratios ranging from 2.5:1 to 200:1

Mod. Ratio	2.5		5		12.5		25		50		100		200	
Coefficient	*H*	*NH*	*H*	*NH*	*H*	*NH*	*H*	*NH*	*H*	*NH*	*H*	*NH*	*H*	*NH*
Regression	0.55	0.72	0.93	1.36	2.19	3.24	4.08	6.21	8.22	11.7	15.4	22.7	30.7	44.5
R Squared	*0.97*	*0.99*	*0.95*	*0.99*	*0.99*	*0.97*	*0.98*	*0.98*	*0.99*	*0.98*	*0.98*	*0.98*	*0.99*	*0.97*

Table 5: Regression and force-based coefficients for a/T_f=0.3 and percentage differences for modulus ratios ranging from 2.5:1 to 200:1

Mod. Ratio	2.5		5		12.5		25		50		100		200	
Coefficient	*H*	*NH*	*H*	*NH*	*H*	*NH*	*H*	*NH*	*H*	*NH*	*H*	*NH*	*H*	*NH*
Regression	0.55	0.72	0.93	1.36	2.19	3.24	4.08	6.21	8.22	11.7	15.4	22.7	30.7	44.5
Force-based	0.53	0.72	0.87	1.37	2.17	3.31	3.96	6.50	8.20	11.6	14.9	22.3	29.9	43.8
% Diff.	*4.8*	*0.1*	*6.0*	*0.8*	*0.8*	*2.2*	*3.0*	*4.4*	*0.2*	*1.1*	*2.9*	*1.7*	*2.5*	*1.6*

To confirm the ability of the regression models to replicate results in the models from which they were derived, the pressure field, *p(r)*, which resulted from the coefficients, was reapplied for modulus ratios of 2.5:1, 5:1, and 100:1. These simulations showed that the coefficients, when reapplied, produced maximum normal stresses, $\sigma_{yy}^{\max}$, to within 5% and maximum displacement values

and to within 1% from the displacement simulations from which they were created. Figure 19 shown below depicts a sample stress profile from the results of reapplying the pressure field to a nonhomogeneous layered case with a modulus ratio of 5:1 and a contact length to film thickness ratio of 0.3.

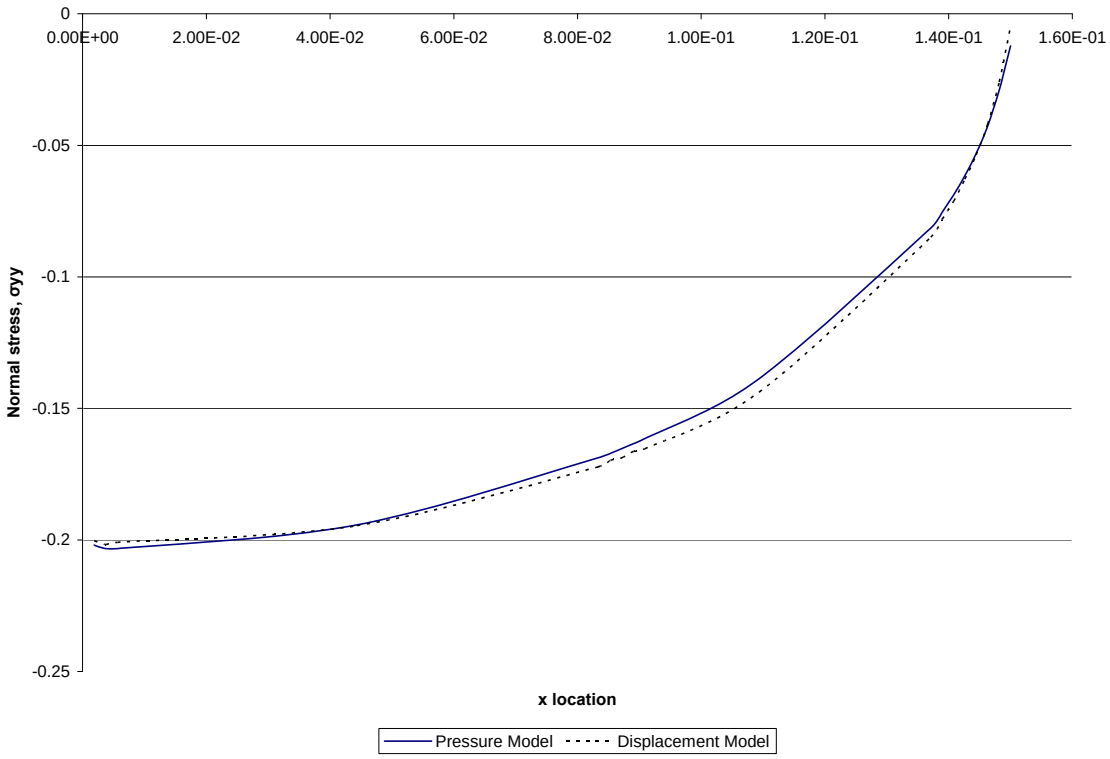

Figure 20: Sample comparison normal stress for the pressure model to displacement model results for a nonhomogeneous modulus ratio of 5:1 across a contact length of 0.15

5.7 Overview of results and discussion

The results of this study suggest that a displacement boundary condition to an indenter produces the same results as a force or pressure distribution boundary condition. The critical normal stresses that occur between modeling a film as a nonhomogeneous and as a homogeneous material vary from 19% for a

modulus ratio of 2.5:1 to as high as 66% for a modulus ratio of 200:1 indicating that the modeling techniques produced very different maximum normal stresses. Additionally, the ratios for maximum displacement and maximum shear stress at the interface also suggest that these modeling techniques produce very different results which become more pronounced as the modulus ratios increase.

The results from the reapplication of the pressure field derived from the regression coefficients and the R^2 values from these regression models indicate the correctness of the regression model used as well as its ability to replicate the critical normal stresses in the contact area and displacements in a FEA model for both the nonhomogeneous and the homogeneous modeling techniques

The agreement between the regression based coefficients and the force-based coefficients suggests the validity for the use of the theoretical axisymmetric Hertzian contact model for defining pressure field in the contact area and displacements for both the homogeneous case and the nonhomogeneous case if the applied force to the indenter is known for contact length to film thicknesses ranging from 0.2 to 0.4.

For the nonhomogeneous case, an increase in the percentage difference between the regression coefficient and the pressure coefficient did not increase from modulus ratios from 2.5:1 to 200:1 indicating that the axisymmetric Hertzian contact model should produce relatively accurate results for normal stresses in this range for functionally gradient materials with linearly varying modulus.

The results from the homogeneous case, due to the average modulus having been used between E_1 and E_2 only suggest the validity of the

axisymmetric Hertzian contact model for modulus ratios ranging from 2.5:1 to 100.5:1 for abrupt interface composites. Like the results from the nonhomogeneous case, there did not appear to be an increase in the percentage difference between the regression based coefficients and the force-based coefficient indicating no trend in the error associated with the results of critical normal stresses at the surface and increasing modulus ratios in this range.

It would be interesting in future studies to examine different modeling techniques for the functionally gradient layer as well as to examine the planar case. While there is a great variation between modeling the film layer as a homogeneous material having the average properties of the film and the substrate and as a linearly varying material, the effects modeling this layer as an exponentially varying material layer and comparing these results to the linear model would be beneficial.

References

Cai, X., Bangert, H., 1996, *Finite-element analysis of the interface influence on hardness measurements of thin films*, Surface and Coatings Technology 81, 240-255.

Chasalani, P., Kaw, A., Daly, J., Nguyen, C., 2007, *Effect of geometrical and material properties in nanoindentation of layered materials with an interphase*, Int. J. Solids Struc, in press.

Chudoba, T., Schwarzer, N., Linss, V., Ritcher, F., 2004. *Determination of mechanical properties of graded coatings using nanoindentation*. Thin Solid Films 239, 469-470.

Chudoba, T., Schwarzer, N., Richter, F., 2000. *Determination of elastic properties if thin films by indentation measurements with a spherical indenter*, Surface and Coating Technology 127, 9-17.

Chudoba, T., Schwarzer, N., Richter, F., 2002. *Steps towards a mechanical modeling of layered systems*, Surface and Coating Technology 154, 140-151.

Diao, D., Kandori A., 2006, *Finite element analysis of the effect of interfacial roughness and adhesion strength on the local delamination of hard coating under sliding contact*. Tribology International 39, 849-855.

Ke, L., Wang, Y., 2006. *Two-dimensional contact mechanics of functionally graded materials with arbitrary spatial variations of material properties*, International Journal of Solids and Structures 43, 5779-5798.

Linss, V., Schwarzer, N., Chudoba, T., Karniychuk, M., Richter F., 2005. *Mechanical properties of a graded B-C-N sputtered coating with varying Young's modulus: deposition, theoretical modeling and nanoindentation.* Surface and Coatings Technology 195, 287-297.

Narayan, R., Hobbs, L. W., Jin, C., Rabiei, A., 2006, *The use of functionally gradient materials in medicine*, JOM 58 (7), 52-56.

Release 10.0 Documentation for ANSYS, 2005, SAS IP, Inc.

Release 10.0 Documentation for ANSYS, 2005, *Static Hertz Contact Problem solved using CONTA178 elements,* ANSYS Verification Manual 63.

Sadeghipour, K., Chen, W., Baran, G., 1994. *Spherical micro-indentation process of polymer-based materials: a finite element study*, J. Phys. D: Appl. Phys. 27, 1300-1310.

Schwarzer, N., Richter, F., and Hecht, G, 1999, *Elastic field in a coated half-space under Hertzian pressure distribution*. Surface and Coating Technology 114, 191-198.

Timoshenko, Goodier, Theory of Elasticity, 3rd Ed., Art. 140.

Vanimisetti, S.K., Narasimhan, R., 2005, A numerical analysis of spherical indentation response of thin hard films on soft substrates, Int. J. Solids Struc., in press.

Appendices

Appendix A: Convergence study and MathCAD worksheets

A.1: Alpha-beta convergence

$$\begin{pmatrix}\sigma_1\\ \sigma_2\\ \sigma_3\end{pmatrix} := \begin{pmatrix}-.165\\ -.2354\\ -.2415\end{pmatrix}$$

$$\begin{pmatrix}N_1\\ N_2\\ N_3\end{pmatrix} := \begin{pmatrix}20\\ 30\\ 40\end{pmatrix}$$

$$\begin{pmatrix}A_c\\ B_c\\ \alpha_c\end{pmatrix} := \begin{pmatrix}-2.4\\ .01\\ .01\end{pmatrix}$$ Initial Guesses

Given

$$\sigma_1 = A_c + \frac{B_c}{N_1^{\alpha_c}} \qquad \sigma_2 = A_c + \frac{B_c}{N_2^{\alpha_c}} \qquad \sigma_3 = A_c + \frac{B_c}{N_3^{\alpha_c}}$$

$$\begin{pmatrix}A_{cs}\\ B_{cs}\\ \alpha_{cs}\end{pmatrix} := \text{Find}\left(A_c, B_c, \alpha_c\right)$$

$$\begin{pmatrix}A_{cs}\\ B_{cs}\\ \alpha_{cs}\end{pmatrix} = \begin{pmatrix}-0.243\\ 2.443\times 10^{6}\\ 5.762\end{pmatrix}$$

Appendix A: (Continued)

$$\begin{pmatrix} \sigma_1 \\ \sigma_2 \\ \sigma_3 \end{pmatrix} := \begin{pmatrix} -3.021 \\ -5.234 \\ -6.530 \end{pmatrix}$$

$$\begin{pmatrix} N_1 \\ N_2 \\ N_3 \end{pmatrix} := \begin{pmatrix} 20 \\ 30 \\ 40 \end{pmatrix}$$

Given

$$\sigma_1 = A_c + \frac{B_c}{N_1^{\alpha_c}} \qquad \sigma_2 = A_c + \frac{B_c}{N_2^{\alpha_c}} \qquad \sigma_3 = A_c + \frac{B_c}{N_3^{\alpha_c}}$$

$$\begin{pmatrix} A_c \\ B_c \\ \alpha_c \end{pmatrix} := \begin{pmatrix} -7.1 \\ .1 \\ 1 \end{pmatrix}$$ Initial Guesses

$$\begin{pmatrix} A_{cs} \\ B_{cs} \\ \alpha_{cs} \end{pmatrix} := \text{Find}\left(A_c, B_c, \alpha_c\right)$$

$$\begin{pmatrix} A_{cs} \\ B_{cs} \\ \alpha_{cs} \end{pmatrix} = \begin{pmatrix} -14.08 \\ 57.567 \\ 0.551 \end{pmatrix}$$

Appendix A: (Continued)

A.2: MathCAD program for force calculations

$S02_{25H} :=$

$SPL_{25H} := cspline\left(xval_{02}, S02_{25H}\right)$

$pfieldH_{25}(x) := interp\left(SPL_{25H}, xval_{02}, S02_{25H}, x\right)$

$len02 := length\left(xval_{02}\right) - 1$

$$P_{25H} := 2\pi\left(\int_{xval_{02_0}}^{xval_{02_{len02}}} pfieldH_{25}(x)\cdot x\,dx\right)$$

$P_{25H} = -6.194\times 10^{-4}$

Appendix B: Element definitions

B.1: CONTA171 full element definition

Release 10.0 Documentation for ANSYS

Element Reference | Part I. Element Library |

CONTA171

2-D 2-Node Surface-to-Surface Contact

MP ME ST <> <> PR EM <> <> PP ED

CONTA171 Element Description

CONTA171 is used to represent contact and sliding between 2-D “target” surfaces (TARGE169) and a deformable surface, defined by this element. The element is applicable to 2-D structural and coupled field contact analyses. This element is located on the surfaces of 2-D solid, shell, or beam elements without midside nodes (PLANE42, PLANE67, PLANE182, VISCO106, SHELL51, SHELL208, BEAM3, BEAM23, PLANE13, PLANE55, or MATRIX50). It has the same geometric characteristics as the solid, shell, or beam element face with which it is connected (see Figure 171.1: "CONTA171 Geometry"). Contact occurs when the element surface penetrates one of the target segment elements (TARGE169) on a specified target surface. Coulomb and shear stress friction is allowed. See CONTA171 in the *ANSYS, Inc. Theory Reference* for more details about this element. Other surface-to-surface contact elements (CONTA172, CONTA173, CONTA174) are also available.

Figure 171.1 CONTA171 Geometry

CONTA171 Input Data

The geometry and node locations are shown in Figure 171.1: "CONTA171 Geometry". The element is defined by two nodes (the underlying solid, shell, or beam element has no

midside nodes). If the underlying solid, shell, or beam elements do have midside nodes, use CONTA172. The element x-axis is along the I-J line of the element. The correct node ordering of the contact element is critical for proper detection of contact. The nodes mustbe ordered such that the target must lie to the right side of the contact element when moving from the first contact element node to the second contact element node as in Figure 171.1: "CONTA171 Geometry". See Generating Contact Elements in the *ANSYS Contact Technology Guide* for more information on generating elements automatically using the ESURF command.

The 2-D contact surface elements are associated with the 2-D target segment elements (TARGE169) via a shared real constant set. ANSYS looks for contact only between surfaces with the same real constant set. For modeling either rigid-flexible or flexible-flexible contact, one of the deformable surfaces must be represented by a contact surface. See Designating Contact and Target Surfaces in the *ANSYS Contact Technology Guide* for more information.

If more than one target surface will make contact with the same boundary of solid elements, you must define several contact elements that share the same geometry but relate to separate targets (targets which have different real constant numbers), or you must combine the two target surfaces into one (targets that share the same real constant numbers).

This element supports various 2-D stress states, including plane stress, plane strain, and axisymmetric states. The stress state is automatically detected according to the stress state of the underlying element. However, if the underlying element is a superelement, you must use KEYOPT(3) to specify the stress state.

A summary of the element input is given in "CONTA171 Input Summary". A general description of element input is given in Element Input. For axisymmetric applications see Axisymmetric Elements.

CONTA171 Input Summary

Nodes
KEYOPTs

> Presented below is a list of KEYOPTS available for this element. Included are links to sections in the *ANSYS Contact Technology Guide* where more information is available on a particular topic.

KEYOPT(1)

> Selects degrees of freedom:

0 --

UX, UY

1 --

UX, UY, TEMP

2 --

TEMP

3 --

UX, UY, TEMP, VOLT

4 --

TEMP, VOLT

5 --

UX, UY, VOLT

6 --

VOLT

7 --

AZ

KEYOPT(2)

Contact algorithm:

0 --

Augmented Lagrangian (default)

1 --

Penalty function

2 --

Multipoint constraint (MPC); see Chapter 8: "Multipoint Constraints and Assemblies" in the *ANSYS Contact Technology Guide* for more information

3 --

Lagrange multiplier on contact normal and penalty on tangent

4 --

Pure Lagrange multiplier on contact normal and tangent

KEYOPT(3)

Stress state when superelements are present:

0 --

Use with h-elements (no superelements)

1 --

Axisymmetric (use with superelements only)

2 --

Plane stress/Plane strain (use with superelements only)

Plane stress with thickness input (use with superelements only)

KEYOPT(4)

Location of contact detection point:

0 --

On Gauss point (for general cases)

1 --

On nodal point - normal from contact surface

2 --

On nodal point - normal to target surface

Use nodal points only for point-to-surface contact.

When using the multipoint constraint (MPC) approach to define surface-based constraints, use KEYOPT(4) in the following way: set KEYOPT(4) = 1 for a force-distributed surface, set KEYOPT(4) = 2 for a rigid constraint surface. See Surface-based Constraints for more information.

KEYOPT(5)

CNOF/ICONT Automated adjustment:

0 --

No automated adjustment

1 --

Close gap with auto CNOF

2 --

Reduce penetration with auto CNOF

3 --

Close gap/reduce penetration with auto CNOF

4 --

Auto ICONT

KEYOPT(6)

Contact stiffness variation (used to enhance stiffness updating when KEYOPT(10) > 0):

0 --

Use default range for stiffness updating

1 --

Make a nominal refinement to the allowable stiffness range

2 --

Make an aggressive refinement to the allowable stiffness range

KEYOPT(7)

Element level time incrementation control:

0 --

No control

1 --

Automatic bisection of increment

2 --

Change in contact predictions made to maintain a reasonable time/load increment

3 --

Change in contact predictions made to achieve the minimum time/load increment whenever a change in contact status occurs

For KEYOPT(7) = 2 or 3, includes automatic bisection of increment. Activated only if SOLCONTROL,ON,ON at the procedure level.

KEYOPT(8)

Asymmetric contact selection:

0 --

No action

2 --

ANSYS internally selects which asymmetric contact pair is used at the solution stage (used only when symmetry contact is defined).

KEYOPT(9)

Effect of initial penetration or gap:

0 --
Include both initial geometrical penetration or gap and offset
1 --

Exclude both initial geometrical penetration or gap and offset

2 --

Include both initial geometrical penetration or gap and offset, but with ramped effects

3 --

Include offset only (exclude initial geometrical penetration or gap)

4 --

Include offset only (exclude initial geometrical penetration or gap), but with ramped effects

For KEYOPT(9) = 1, 3, or 4, the indicated initial gap effect is considered only if KEYOPT(12) = 4 or 5.

KEYOPT(10)

Contact stiffness update:

0 --

Each load step if FKN is redefined during load step (pair based).

1 --

Each substep based on mean stress of underlying elements from the previous substep (pair based).

2 --

Each iteration based on current mean stress of underlying elements (pair based).

3 --

Each load step if FKN is redefined during load step (individual element based).

4 --

Each substep based on mean stress of underlying elements from the previous substep (individual element based).

5 --

Each iteration based on current mean stress of underlying elements (individual element based).

KEYOPT(10) = 0, 1, and 2 are pair based, meaning that the stiffness and settings for ICONT, FTOLN, PINB, PMAX, and PMIN are averaged across all the contact elements in a contact pair. For KEYOPT(10) = 3, 4, and 5, the stiffness and settings are based on each individual contact element (geometry and material behaviors).

KEYOPT(11)

Beam/Shell thickness effect:

0 --

Exclude

1 --

Include

KEYOPT(12)

Behavior of contact surface:

0 --

Standard

1 --

Rough

2 --

No separation (sliding permitted)

3 --

Bonded

4 --

No separation (always)

5 --

Bonded (always)

6 --

Bonded (initial contact)

CONTA171 Output Data

The solution output associated with the element is in two forms:

- Nodal displacements included in the overall nodal solution
- Additional element output as shown in Table 171.2: "CONTA171 Element Output Definitions"

A general description of solution output is given in Solution Output. See the *ANSYS Basic Analysis Guide* for ways to view results.

The Element Output Definitions table uses the following notation:

A colon (:) in the Name column indicates the item can be accessed by the Component Name method [ETABLE, ESOL]. The O column indicates the availability of the items in the file `Jobname.OUT`. The R column indicates the availability of the items in the results file.

In either the O or R columns, Y indicates that the item is *always* available, a number refers to a table footnote that describes when the item is *conditionally* available, and a - indicates that the item is *not* available.

Table 171.2: "CONTA171 Element Output Definitions" gives element output. In the results file, the nodal results are obtained from its closest integration point.

- The 2-D contact element must be defined in an X-Y plane and the Y-axis must be the axis of symmetry for axisymmetric analyses.
- An axisymmetric structure should be modeled in the +X quadrants.
- This 2-D contact element works with any 3-D elements in your model.
- Do not use this element in any model that contains axisymmetric harmonic elements.
- Node numbering must coincide with the external surface of the underlying solid, shell, or beam element, or with the original elements comprising the superelement.
- This element is nonlinear and requires a full Newton iterative solution, regardless of whether large or small deflections are specified.
- The normal contact stiffness factor (FKN) must not be so large as to cause numerical instability.
- FTOLN, PINB, and FKOP can be changed between load steps or during restart stages.
- The value of FKN can be smaller when combined with the Lagrangian multiplier method, for which FTOLN must be used.
- You can use this element in nonlinear static or nonlinear full transient analyses. In addition, you can use it in modal analyses, eigenvalue buckling analyses, and harmonic analyses. For these analysis types, the program assumes that the initial status of the element (i.e., the status at the completion of the static prestress analysis, if any) does not change.

- When nodal detection is used and the contact node is on the axis of symmetry in an axisymmetric analysis, the contact pressure on that node is not accurate since the area of the node is zero. The contact force is accurate in this situation.
- This element allows birth and death and will follow the birth and death status of the underlying solid, shell, beam, or target elements.

CONTA171 Product Restrictions

When used in the product(s) listed below, the stated product-specific restrictions apply to this element in addition to the general assumptions and restrictions given in the previous section.

ANSYS Professional.

- The MU material property is not allowed.
- The birth and death special feature is not allowed.
- The DAMP material property is not allowed.

ANSYS Structural.

- The VOLT DOF (KEYOPT(1) = 3 through 6) is not allowed.
- The AZ DOF (KEYOPT(1) = 7) is not allowed.

ANSYS Mechanical.

- The AZ DOF (KEYOPT(1) = 7) is not allowed.

B.2 TARGE169 full element definition

Release 10.0 Documentation for ANSYS

Element Reference | Part I. Element Library |

TARGE169

2-D Target Segment

MP ME ST <> <> PR EM <> <> PP ED

TARGE169 Element Description

TARGE169 is used to represent various 2-D "target" surfaces for the associated contact elements (CONTA171, CONTA172, and CONTA175). The contact elements themselves overlay the solid elements describing the boundary of a deformable body and are potentially in contact with the target surface, defined by TARGE169. This target surface is discretized by a set of target segment elements (TARGE169) and is paired with its associated contact surface via a shared real constant set. You can impose any translational or rotational displacement, temperature, voltage, and magnetic potential on the target segment element. You can also impose forces and moments on target elements. See TARGE169 in the *ANSYS, Inc. Theory Reference* for more details about this element. To represent 3-D target surfaces, use TARGE170, a 3-D target segment element. For rigid targets, these elements can easily model complex target shapes. For flexible targets, these elements will overlay the solid elements describing the boundary of the deformable target body.

Figure 169.1 TARGE169 Geometry

TARGE169 Input Data

The target surface is modeled through a set of *target segments,* typically, several target segments comprise one target surface.

The target surface can either be rigid or deformable. For modeling rigid-flexible contact, the rigid surface must be represented by a target surface. For flexible-flexible contact, one of the deformable surfaces must be overlayed by a target surface. See the *ANSYS Contact Technology Guide* for more information about designating contact and target surfaces.

The target and associated contact surfaces are identified by a shared real constant set. This real constant set includes all real constants for both the target and contact elements.

Each target surface can be associated with only one contact surface, and vice-versa. However, several contact elements could make up the contact surface and thus come in contact with the same target surface. Likewise, several target elements could make up the target surface and thus come in contact with the same contact surface. For either the target or contact surfaces, you can put many elements in a single target or contact surface,

but doing so may increase computational cost. For a more efficient model, localize the contact and target surfaces by splitting the large surfaces into smaller target and contact surfaces, each of which contain fewer elements.

If one contact surface may contact more than one target surface, you must define duplicate contact surfaces that share the same geometry but relate to separate targets, that is, have separate real constant set numbers.

For any target surface definition, the node ordering of the target segment element is critical for proper detection of contact. The nodes must be ordered so that, for a 2-D surface, the associated contact elements (CONTA171, CONTA172, or CONTA175) must lie to the right of the target surface when moving from target node I to target node J. For a rigid 2-D complete circle, contact must occur on the outside of the circle; internal contacting is not allowed.

Considerations for Rigid Targets

Each target segment is a single element with a specific shape, or *segment type*. The segment types are defined by one, two, or three nodes and a target shape code,

TSHAP, and are described in Table 169.1: "TARGE169 2-D Segment Types, Target Shape Codes, and Nodes". The TSHAP command indicates the geometry (shape) of the element. The segment dimensions are defined by a real constant (R1), and the segment location is determined by the nodes. ANSYS supports six 2-D segment types; see Table 169.1: "TARGE169 2-D Segment Types, Target Shape Codes, and Nodes".

1. The DOF available depends on the setting of KEYOPT(1) for the associated contact element. For more information, see the element documentation for CONTA171, CONTA172, or CONTA175.
2. When creating a circle via direct generation, define the real constant R1 *before* creating the element.

Figure 169.2 TARGE169 2-D Segment Types

For simple rigid target surfaces, you can define the target segment elements individually by direct generation. You must first specify the *SHAPE* argument for the TSHAP command. When creating circles through direct generation, you must also define the real constant R1 before creating the element. Real constant R1 (see Table 169.1: "TARGE169 2-D Segment Types, Target Shape Codes, and Nodes") defines the radius of the target circle.

For general 2-D rigid surfaces, target segment elements can be defined by line meshing (LMESH). You can also use keypoint meshing (KMESH) to generate the pilot node.

If the TARGE169 elements will be created via automatic meshing (LMESH or KMESH), then the TSHAP command is ignored and ANSYS chooses the correct shape automatically.

The pilot node provides a convenient, powerful way to assign boundary conditions such as rotations, translations, moments, temperature, and voltage on an entire rigid target surface. You assign the conditions only to the pilot node, eliminating the need to assign boundary conditions to individual nodes and reducing the chance of error. The pilot node, unlike the other segment types, is used to define the degrees of freedom for the entire target surface. This node can be any of the target surface nodes, but it does not have to be. All possible rigid motions of the target surface will be a combination of a translation and a rotation around the pilot node. The boundary conditions (including displacement, rotation, force, moment, temperature, voltage, and magnetic potential) of the entire target surface can be specified only on pilot nodes.

For rotation of a rigid body constrained only by a bonded, rigid-flexible contact pair with a pilot node, use the MPC algorithm or a surface-based constraint as described in Multipoint Constraints and Assemblies. Penalty-based algorithms can create undesirable rotational energies in this situation.

By default, ANSYS automatically fixes the degree of freedom for rigid target nodes if they aren't explicitly constrained (KEYOPT(2) = 0). If you wish, you can override the automatic boundary condition settings by setting KEYOPT(2) = 1.

By default, the temperature is set to the value of TUNIF, and if this has no explicit value the temperature is set to zero. For thermal contact analysis, such as convection and radiation modeling, the behavior of a thermal contact surface (whether a “near-field” or “free” surface) is usually based on the contact status. Contact status affects the behavior of the contact surface as follows:

- If the contact surface is outside the pinball region, its behavior is as a far-field of free surface. In this instance, convection/radiation occurs with the ambient temperature.
- If the contact surface is inside the pinball region, the behavior is as a near-field surface.

However, the thermal contact surface status is ignored if KEYOPT(3) = 1 is set, and the surface is always treated as a free surface (see CONTA171, CONTA172, or CONTA175 for details).

Considerations for Deformable Target Surfaces

For general deformable surfaces, you will normally use the ESURF command to overlay the target elements on the boundary of the existing mesh. Note that the segment types (TSHAP command) should not be used for this case.

A summary of the element input is given in "TARGE169 Input Summary". A general description of element input is given in Element Input.

TARGE169 Input Summary

Nodes

I, J, K (J and K are not required for all segment types)

Degrees of Freedom

UX, UY, ROTZ, TEMP, VOLT, AZ (ROTZ is used for the pilot node only)

Real Constants

R1, R2, [the others are defined through the associated CONTA171, CONTA172, or CONTA175 element]

Material Properties

None

Surface Loads

None

Body Loads

None

Special Features

Nonlinear

Birth and death

KEYOPT(2)

Boundary conditions for rigid target nodes:

0 --

Automatically constrained by ANSYS

1 --

Specified by user

KEYOPT(3)

Behavior of thermal contact surface

0 --

Based on contact status

Treated as free-surface

KEYOPT(4)

DOF set to be constrained on dependent DOF for internally-generated multipoint constraints (MPCs), used only for a surface-based constraint where a single pilot node is used for the target element (see Surface-Based Constraints in the *ANSYS Contact Technology Guide* for more information):

n --

Enter a three digit value that represents the DOF set to be constrained. The first to third digits represent ROTZ, UY, UX, respectively. The number 1 (one) indicates the DOF is active, and the number 0 (zero) indicates the DOF is not active. For example, 011 means that UX and UY will be used in the multipoint constraint. Leading zeros may be omitted; for example, you can enter 1 to indicate that UX is the only active DOF. If KEYOPT(4) = 0 (which is the default) or 111, all DOF are constrained.

TARGE169 Output Data

The solution output associated with the element is shown in Table 169.2: "TARGE169 Element Output Definitions". The following notation is used:

The Element Output Definitions table uses the following notation:

A colon (:) in the Name column indicates the item can be accessed by the Component Name method [ETABLE, ESOL]. The O column indicates the availability of the items in the file `Jobname.OUT`. The R column indicates the availability of the items in the results file.

In either the O or R columns, Y indicates that the item is *always* available, a number refers to a table footnote that describes when the item is *conditionally* available, and a - indicates that the item is *not* available.

1. Determined by ANSYS

TARGE169 Assumptions and Restrictions

- The 2-D segment element must be defined in an X-Y plane.
- For circular arcs, the third node defines the actual center of the circle and must be defined accurately when the element is generated and must be moved consistently with the other nodes during the deformation process. If the third node is not moved consistently with the other nodes, the arc shape will change with that node's movement. To ensure the correct behavior, apply all boundary conditions to a pilot node.
- For parabolic segments, the third point must lie at the middle of the parabola.
- For rigid surfaces, no external forces can be applied on target nodes except on a pilot node. If a pilot node is specified for a target surface, ANSYS will ignore the boundary conditions on any nodes of the target surface except for the pilot nodes. For each pilot node, ANSYS automatically defines an internal node and an internal constraint equation. The rotational DOF of the pilot node is connected to the translational DOF of the internal node by the internal constraint equation. You cannot use constraint equations or coupling on pilot nodes.
- Generally speaking, you should not change the R1 real constant between load steps or during restart stages; otherwise ANSYS assumes the radius of the circle varies between the load steps. When using direct generation, the real constant R1 for circles may be defined before the input of the element nodes. If multiple rigid

- circles are defined, each having a different radius, they must be defined by different target surfaces.

TARGE169 Product Restrictions

There are no product-specific restrictions for this element.